

IS GRAPH CONVOLUTION ALWAYS BENEFICIAL FOR EVERY FEATURE?

Anonymous authors

Paper under double-blind review

ABSTRACT

Graph Neural Networks (GNNs) have demonstrated strong capabilities in processing structured data. While traditional GNNs typically treat each feature dimension equally during graph convolution, we raise an important question: *Is the graph convolution operation equally beneficial for each feature?* If not, the convolution operation on certain feature dimensions can possibly lead to harmful effects, even worse than the convolution-free models. Traditional feature selection methods focus on identifying informative features or reducing redundancy, but they are not suitable for structured data since they overlook graph structures. In the context of graphs, few studies have investigated GNN performance concerning node features using feature homophily metrics, which assess feature consistency with graph topology. Unfortunately, these metrics have not effectively aligned with GNN performance or served as reliable guides for feature selection in GNNs. To address these limitations, we introduce a novel metric, Topological Feature Informativeness (TFI), to distinguish between GNN-favored and GNN-disfavored features, where its effectiveness is validated through both theoretical analysis and empirical observations. Based on TFI, we propose a simple yet effective Graph Feature Selection (GFS) method, which processes GNN-favored and GNN-disfavored features separately, using GNNs and non-GNN models. Compared to original GNNs, GFS significantly improves the extraction of useful topological information from each feature with comparable computational costs. Extensive experiments show that after applying GFS to 8 baseline and state-of-the-art (SOTA) GNN architectures across 10 datasets, 90% of the GFS-augmented cases show significant performance boosts. Furthermore, our proposed TFI metric outperforms other feature selection methods in graphs. These results validate the effectiveness of both GFS and TFI. Additionally, we demonstrate that GFS’s improvements are robust to hyperparameter tuning, highlighting its potential as a universal method for enhancing various GNN architectures.

1 INTRODUCTION

Graph Neural Networks (GNNs) are widely used for processing graph-structured data, such as recommendation systems (Wu et al., 2022; 2019b), social networks (Li et al., 2023a; Awasthi et al., 2023; Luan et al., 2019), telecommunication (Lu et al., 2024a) and bio-informatics (Zhang et al., 2021; Kang et al., 2022; Hua et al., 2024). Although graph convolution has been shown effective to enrich node features with topological information through message propagation, the performance gain is found to be restricted by the assumption of homophily, *i.e.*, similar nodes are more likely to be connected in a graph (McPherson et al., 2001). On the other hand, when a graph exhibits low homophily, *i.e.*, heterophily, the graph convolution operation can lead to performance degradation and sometimes even underperform convolution-free models, such as Multi-Layer Perceptrons (MLPs) (Zhu et al., 2020a; Luan et al., 2022b; 2024c). Therefore, to measure the impact of graph convolution operation, label-based homophily metrics (Pei et al., 2020a; Zhu et al., 2020a) are proposed to measure the label consistency along graph topology. However, they neglect the effects on node features, which is crucial for graph learning. Feature homophily metrics (Yang et al., 2021a; Jin et al., 2022) are then proposed to measure the feature consistency along the graph.

Although these existing metrics can capture the feature similarity between connected nodes, they overlook that different feature dimensions may exhibit different levels of compatibility with graph

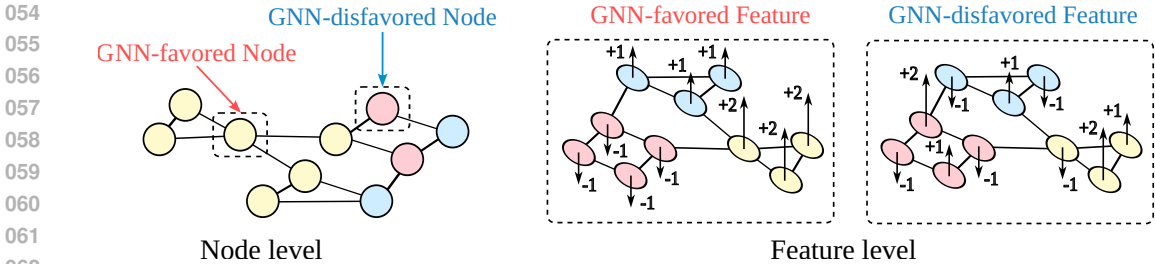


Figure 1: Improvements in GNN performance at node level and feature level. Different colors denote node labels, while the direction and magnitude of arrows denote node features.

structures, and thus may gain different amounts of benefits or negative impacts from graph convolution. For example, as illustrated in Figure 1 (right), the GNN-favored feature exhibits uniform values among intra-class nodes while differing across inter-class nodes. This characteristic enables graph convolution operation to effectively improve the distinguishability among nodes from different classes, as demonstrated in (Luan et al., 2024b). Conversely, graph convolution on GNN-disfavored features may hinder the learning process of GNNs. This example raises a crucial question: *How can we determine whether graph convolution is beneficial or not for a specific feature?*

To address this issue, in this paper, we propose **Topological Feature Informativeness (TFI)**, which measures the mutual information between each dimension of aggregated node features and labels. Compared with previous feature selection metrics [1] that primarily focused on selecting the most informative features or reducing redundancy for *i.i.d.* data, our proposed TFI emphasizes differentiating between GNN-favored and GNN-disfavored features, which is essential for effective graph representation learning. Specifically, TFI can identify features that are either favored or disfavored by GNNs, provably providing an upper bound on the performance gap between graph convolution and convolution-free models, which is then supported by both theoretical analysis and empirical observations. Additionally, TFI overcomes the “good heterophily” issue (Ma et al., 2021), which is a serious misalignment of existing feature homophily metrics and GNN performance.

Motivated by the principle of “feed the right features to the right model” Luan et al. (2022a), we propose a simple yet effective method called **Graph Feature Selection (GFS)**. GFS first uses TFI to identify GNN-favored and GNN-disfavored features. Then, to enhance the extraction of useful information, the GNN-favored features are processed by GNNs, while MLPs handle the GNN-disfavored features. Last, a final linear layer fuses the embeddings from both models to obtain the final node representation. GFS can be seamlessly integrated into almost any GNN architecture, improving overall model performance with comparable computational costs. Our experiments on real-world datasets demonstrate that GFS significantly boosts the performance of 8 GNNs across 10 datasets in node classification tasks and the improvement is robust to hyperparameter tuning. Moreover, we demonstrate that TFI outperforms other statistical and optimization-based metrics for feature selection in GNNs, validating its superiority. Besides, we surprisingly find that GFS is much more effective on node embeddings encoded by Pretrained Large Models (PLMs) than other methods. This implies that the advantages of PLMs in understanding graph-structured data might be rooted in their ability to disentangle the topology-aware and topology-agnostic information into separate feature dimensions. In summary, our main contributions are as follows.

- We introduce a novel metric, Topological Feature Informativeness (TFI), to distinguish between GNN-favored and GNN-disfavored features. We validate its effectiveness through both empirical observations and theoretical analysis.
- We propose Graph Feature Selection (GFS) based on TFI, a simple yet powerful method that significantly boosts GNN performance. To the best of our knowledge, this is the first study to address the feature selection problem based on GNN-favored and GNN-disfavored disentanglement.
- Our extensive experiments demonstrate that applying GFS to 8 baseline and state-of-the-art (SOTA) GNN architectures across 10 datasets yields a significant performance boost in 90% (72 out of 80) of the cases.

2 PRELIMINARY

We define a graph as $\mathcal{G} = \{\mathcal{V}, \mathcal{E}\}$, where \mathcal{V} is the node set and \mathcal{E} is the edge set. For an undirected graph, its structure can be represented by an adjacency matrix $\mathbf{A} \in \mathbb{R}^{N \times N}$, where N is the number of nodes, $A_{u,v} = A_{v,u} = 1$ indicates the presence of an edge between nodes u and v , i.e., $e_{uv}, e_{vu} \in \mathcal{E}$, otherwise $A_{u,v} = A_{v,u} = 0$. The node classification task on graph aims to predict node labels $\mathbf{Y} \in \mathbb{R}^N$ by utilizing node features $\mathbf{X} \in \mathbb{R}^{N \times M}$ and topological information, where $X_{u,m}$ denotes the m -th feature of node u . The node degree matrix is denoted as $\mathbf{D} \in \mathbb{R}^{N \times N}$, where $D_u = \sum_{v \in \mathcal{V}} A_{u,v}$ is the degree of node u . The adjacency matrix can be normalized as $\hat{\mathbf{A}} = \mathbf{D}^{-\frac{1}{2}} \mathbf{A} \mathbf{D}^{-\frac{1}{2}}$. The neighbors of node u are denoted by $\mathcal{N}_u = \{v | e_{uv} \in \mathcal{E}\}$.

Graph Neural Networks. Graph Neural Networks (GNNs), such as GCN (Kipf & Welling, 2016), GAT (Velicković et al., 2017), and GraphSage (Hamilton et al., 2017), can effectively capture useful topological information from neighbors by message propagation mechanism. Specifically, for a node u , its embedding z_u^l in the l -th layer of a GNN can be expressed as:

$$z_u^l = \text{UPDATE}(z_u^{l-1}, \text{AGGREGATE}(z_u^{l-1}, \{z_v^{l-1} | v \in \mathcal{N}_u\})) \quad (1)$$

where $\text{AGGREGATE}(\cdot)$ represents the aggregation function, and $\text{UPDATE}(\cdot)$ is the update function based on the ego node and the aggregated neighbor representations from the previous layer. For the first layer, the initial embedding is set as input node features.

The representative graph convolution can be formulated as $\mathbf{H}^l = \sigma(\hat{\mathbf{A}}\mathbf{H}^{l-1}\mathbf{W}^{l-1})$, where \mathbf{H}^l and \mathbf{W}^l denote the node embeddings and learnable parameter matrix at the l -th layer, and $\sigma(\cdot)$ is an activation function. To boost GNN performance, some architectures concatenate ego and neighborhood node embeddings as the input of the next layer (Abu-El-Haija et al., 2019; Zhu et al., 2020b), i.e., $[\hat{\mathbf{A}}\mathbf{H}^{l-1}, \mathbf{H}^{l-1}]$ or adding the aggregated node embeddings with the ego node embeddings (Bo et al., 2021; Luan et al., 2022a), i.e., $(\hat{\mathbf{A}} + \mathbf{I})\mathbf{H}^{l-1}$, which has been shown to improve GNN performance (Platonov et al., 2023), especially in the scenario of heterophily (Luan et al., 2024c; Lu et al., 2024b).

Label Homophily. Homophily, a concept originating from social networks, is defined as the tendency of similar nodes are more likely to connect with each other (Khanam et al., 2023). In graph learning, homophily is used to measure whether graph convolution on certain graph is beneficial for GNN or not. Higher homophily implies that the topological structure can provide useful information, which typically leads to better GNN performance. The commonly used label-based homophily metrics are defined as follows:

$$h_{\text{edge}}(\mathcal{G}, \mathbf{Y}) = \frac{|\{e_{uv} | e_{uv} \in \mathcal{E}, Y_u = Y_v\}|}{|\mathcal{E}|}, \quad h_{\text{node}}(\mathcal{G}, \mathbf{Y}) = \frac{1}{|\mathcal{V}|} \sum_{v \in \mathcal{V}} \frac{|\{u | u \in \mathcal{N}_v, Y_u = Y_v\}|}{|\mathcal{N}_v|} \quad (2)$$

Generally, these metrics only measure label consistency across graph topology, but they overlook the feature aspect, which also plays a critical role in GNN performance (Zheng et al., 2024a). Therefore, some studies focus on the feature consistency across graph topology.

Feature Homophily. To extend the conventional definition of label homophily to node features, feature homophily metrics are introduced. The general form of feature homophily is,

$$h(\mathcal{G}, \mathbf{X};:,m) = \frac{1}{\eta(\mathbf{X};:,m)} \sum_{e_{uv} \in \mathcal{E}} \text{sim}(X_{u,m}, X_{v,m}) \quad (3)$$

where $\eta(\cdot)$ is a normalization function and $\text{sim}(\cdot)$ is a similarity metric. The key difference between different feature homophily metrics lies in the choice of the similarity function $\text{sim}(\cdot)$, which could be cosine similarity (Jin et al., 2022), dot-product (Yang et al., 2021b), or Euclidean distance (Chen et al., 2023). Please refer to Appendix A for more detailed introduction to homophily metrics.

Mutual Information. Mutual Information measures the amount of information obtained about one random variable given another variable (Reza, 1994). More specifically, given variable X and

162 Y , the mutual information can be expressed as¹:

$$163 \quad I(X; Y) = \sum_{y \in \mathcal{Y}} \sum_{x \in \mathcal{X}} p(x, y) \log \frac{p(x, y)}{p(x)p(y)} \quad (4)$$

164 where $p(x, y)$ is joint probability, and $p(x)$ and $p(y)$ are marginal probability distributions.

165 3 TOPOLOGICAL FEATURE INFORMATIVENESS

166 As illustrated in Figure 1, not all features in graphs benefit from graph convolution. This raises
167 the question: how can we determine which features are beneficial for graph convolution? Previ-
168 ous studies (Zheng et al., 2024a; Luan et al., 2024b; Wang et al., 2024a) have demonstrated that
169 it is the stable topological patterns of intra-class nodes that enable effective message aggregation
170 from neighbors, rather than relying solely on consistency-based homophily metrics. To address the
171 limitations of feature homophily metrics, we propose **TFI** (Topological Feature Informativeness) to
172 measure the informativeness of neighbors in graphs given the feature $\mathbf{X}_{:,m}$, which can be expressed
173 as:

$$174 \quad \text{TFI}_m = I(Y; \tilde{\mathbf{X}}_{:,m}) \quad (5)$$

175 where $\tilde{\mathbf{X}}_{:,m} = (\hat{\mathbf{A}})^k \mathbf{X}_{:,m}$ is the aggregated node features from k -hop neighbors. Here $\hat{\mathbf{A}}$ is the
176 adjacency matrix without self-loop, and we set $k = 1$ in $\tilde{\mathbf{X}}_{:,m}$ by default.

177 The proposed TFI_m leverages mutual information to quantify the degree of dependence between
178 variables, thereby revealing both linear and non-linear relationships. Then, we conduct a theoretical
179 analysis to determine how TFI_m can effectively measure whether specific features in graphs benefit
180 from graph convolution.

181 **Theorem 1.** Given a graph $\mathcal{G} = \{\mathcal{V}, \mathcal{E}\}$ with C classes and TFI_m measured on m -th feature, the
182 prediction accuracy P_A of a classifier on node labels \mathbf{Y} with aggregated features $\tilde{\mathbf{X}}_{:,m}$ is upper
183 bounded by:

$$184 \quad P_A \leq \frac{\text{TFI}_m + \log 2}{\log C} \quad (6)$$

185 where the proof is given in Appendix B.

186 From Theorem 1, we can see that TFI_m can measure the effect of graph convolution on feature
187 dimension m by relating it to model performance. More specifically, a higher TFI_m means the
188 prediction accuracy of a classifier with aggregated node feature m has a higher upper bound, which
189 indicates that the graph convolution operation is more likely to be beneficial to feature m . To guide
190 feature selection with TFI_m , we next explain how it relates to the performance gap between graph-
191 convoluted and convolution-free features.

192 **Theorem 2.** The gap between $I(Y; \tilde{\mathbf{X}}_{:,m}, \mathbf{X}_{:,m})$ and $I(Y; \mathbf{X}_{:,m})$ is upper bounded by TFI_m :

$$193 \quad I(Y; \tilde{\mathbf{X}}_{:,m}, \mathbf{X}_{:,m}) - I(Y; \mathbf{X}_{:,m}) = I(Y; \tilde{\mathbf{X}}_{:,m} | \mathbf{X}_{:,m}) \leq I(Y; \tilde{\mathbf{X}}_{:,m}) = \text{TFI}_m \quad (7)$$

194 In Theorem 2, the mutual information $I(Y; \mathbf{X}_{:,m})$ measures how well the ego node features capture
195 the relevant information of labels, without making assumptions about the underlying data distribu-
196 tion. This makes $I(Y; \mathbf{X}_{:,m})$ a non-parametric measure of MLP performance. On the other hand,
197 $I(Y; \tilde{\mathbf{X}}_{:,m}, \mathbf{X}_{:,m})$ serves as a non-parametric measure of GNN performance, which utilizes both
198 the ego node features $\mathbf{X}_{:,m}$ and the aggregated features $\tilde{\mathbf{X}}_{:,m}$ for prediction². The subtraction
199 of $I(Y; \tilde{\mathbf{X}}_{:,m}, \mathbf{X}_{:,m})$ and $I(Y; \mathbf{X}_{:,m})$ indicates the performance gap between graph-convoluted and
200 convolution-free features, which is upper bounded by TFI_m .

201 ¹For a discrete variable Y and a continuous variable X , mutual information is estimated based on entropy
202 using k -nearest neighbor distances, following Kraskov et al. (2004); Ross (2014).

203 ²The combination of $\tilde{\mathbf{X}}_{:,m}$ and $\mathbf{X}_{:,m}$ could be either concatenating node embeddings, *i.e.*, $[\hat{\mathbf{A}}\mathbf{H}^{l-1}, \mathbf{H}^{l-1}]$
204 or adding the aggregated node embeddings with the ego node embeddings, *i.e.*, $(\hat{\mathbf{A}} + \mathbf{I})\mathbf{H}^{l-1}$ as introduced in
205 Section 2

216
217
218
219
220
221
222
223
224
225
226

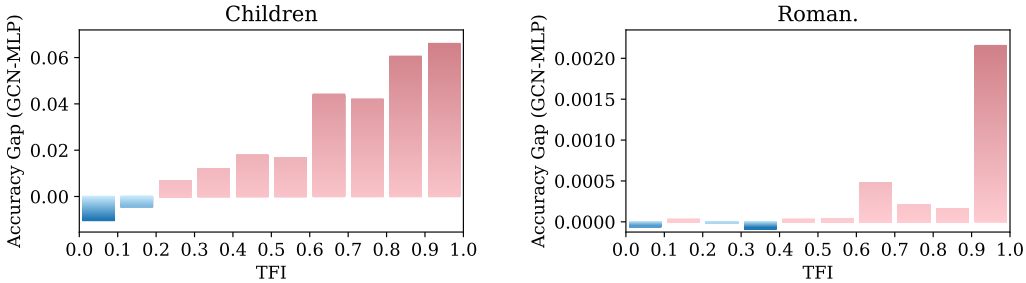


Figure 2: The performance gap between GCN and MLP with the increase of TFI.

227
228
229
230
231
232
233
234
235
236
237
238
239
240

To verify the effectiveness of the above claims about TFI, we conduct experiments on real-world benchmark datasets. Specifically, we first compute TFI_m for all features in the graph, sort them, and divide them evenly into 10 bins. Next, we train GCN and MLP only with the features in a bin respectively, and report the performance difference of GCN and MLP. As shown in Figure 2, GCN underperforms MLP in bins with low TFI and outperforms MLP in bins with high TFI. This observation is consistent with Theorem 1 and 2, and indicates that TFI can effectively identifies GNN-favored and GNN-disfavored features.

Note that the estimation of TFI_m does not require all of the labels Y . In a semi-supervised setting, TFI_m can be calculated using only the training labels and features, *i.e.*, $I(Y_{train}; \hat{X}_{train,m})$, without the need for pseudo labels. In the next section, we will introduce how to use TFI_m for feature selection in GNNs.

4 GRAPH FEATURE SELECTION

241
242
243
244
245
246

In this section, we propose GFS (Graph Feature Selection), a TFI-based feature selection method. It is composed of three main components: (1) GNN-favored feature selection, (2) feature embedding, and (3) feature fusion.

247
248
249
250
251
252
253
254
255
256
257
258
259

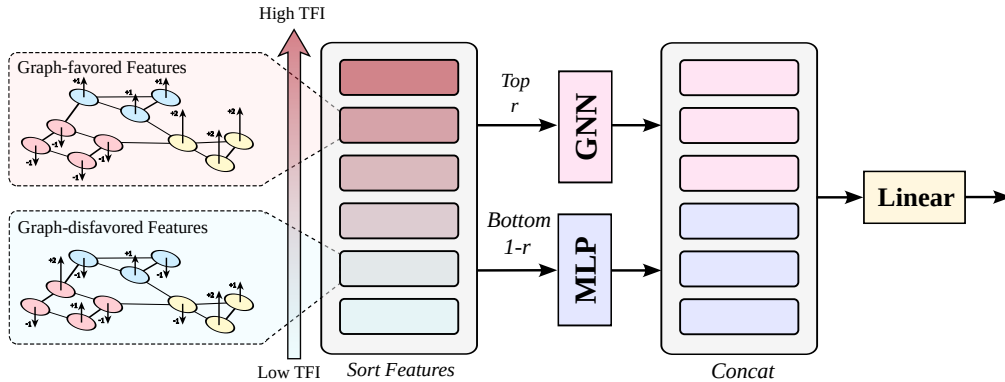


Figure 3: Framework of GFS with TFI.

260
261
262
263
264
265
266
267
268
269

As illustrated in Figure 3, for each feature dimension m , we first measure its corresponding TFI_m using Eq. (5). Since a higher TFI_m indicates stronger GNN performance compared to MLP, we apply a threshold to select the set of **GNN-favored** features as $\{X_G | X_{:,m} \in X_G, TFI_m \geq \delta(r)\}$, where $\delta(r)$ is the threshold corresponding to the top r percentile of all TFI values in features, and $r \in (0, 1)$. The **GNN-disfavored** features are the remaining $1 - r$ of features, defined as $X_{-G} = X \setminus \{X_G\}$.

The GNN-favored features X_G are expected to be more suitable for GNNs, whereas the GNN-disfavored features X_{-G} are better suited for MLPs. Thus, we feed X_G into a GCN (or any other GNN architecture) and X_{-G} into an MLP to better leverage information from both neighbors and

ego nodes. Specifically, in l -th layer of GCN or MLP, we have:

$$\text{GCN: } \mathbf{H}_{\mathcal{G}}^l = \sigma(\hat{\mathbf{A}}\mathbf{H}_{\mathcal{G}}^{l-1}\mathbf{W}_1^{l-1}), \text{ MLP: } \mathbf{H}_{-\mathcal{G}}^l = \sigma(\mathbf{H}_{-\mathcal{G}}^{l-1}\mathbf{W}_2^{l-1}) \quad (8)$$

where $\mathbf{H}_{\mathcal{G}}^0 = \mathbf{X}_{\mathcal{G}}^0$ and $\mathbf{H}_{-\mathcal{G}}^0 = \mathbf{X}_{-\mathcal{G}}^0$. During message passing, the representations of $\mathbf{H}_{\mathcal{G}}^l$ and $\mathbf{H}_{-\mathcal{G}}^l$ are derived independently, ensuring that $\mathbf{X}_{\mathcal{G}}^l$ and $\mathbf{X}_{-\mathcal{G}}^l$ can be encoded by the most appropriate model without interference.

Lastly, to combine the node information from $\mathbf{X}_{\mathcal{G}}$ and $\mathbf{X}_{-\mathcal{G}}$ together, we concatenate the node representation from the last layer L of GNN and MLP, and feed them into a linear layer:

$$\mathbf{H} = [\mathbf{H}_{\mathcal{G}}^L, \mathbf{H}_{-\mathcal{G}}^L]\mathbf{W} + \mathbf{b} \quad (9)$$

where \mathbf{H} is the final node representation, \mathbf{W} is the weight matrix, and \mathbf{b} is the bias, respectively. This final node representation is then used for downstream graph tasks.

Complexity Analysis. To compare the time complexity of GNN+GFS against standard GNNs, we use GCN as the backbone GNN and assume the embedding size F is consistent across all layers. First, estimating and sorting TFI introduces a complexity of $O(KC + N(1 + \log N))$, where K is a parameter related to mutual information estimation, C is the number of classes, and N is the number of nodes. Both K and C are much smaller than N or the number of edges $|\mathcal{E}|$, making this overhead negligible compared to GNN training complexity as below.

After feature selection, we obtain GNN-favored features $\mathbf{X}_{\mathcal{G}} \in \mathbb{R}^{N \times \lceil rM \rceil}$ and GNN-disfavored features $\mathbf{X}_{-\mathcal{G}} \in \mathbb{R}^{N \times \lfloor (1-r)M \rfloor}$, where $\lfloor \cdot \rfloor$ is the floor function. For the first layer of GCN+GFS, the time complexity is $O(|\mathcal{E}| \lceil rM \rceil + N \lceil rM \rceil F)$ for the GNN channel and $O(N \lfloor (1-r)M \rfloor F)$ for the MLP channel. The sum of these terms, $O(|\mathcal{E}| \lceil rM \rceil + NM^2)$, is smaller than the complexity of a standard GCN, $O(|\mathcal{E}|M + NM^2)$, for $r < 1$. This is because GFS reduces the dimension of features that input into GCN.

In subsequent layers, GCN+GFS has a complexity of $O(|\mathcal{E}|F + 2NF^2)$, slightly higher than the complexity of GCN $O(|\mathcal{E}|F + NF^2)$ by an additional NF^2 term due to the MLP layers. However, this additional cost $O(NF^2)$ is smaller than the $O(|\mathcal{E}|F)$ introduced by graph convolutions. Thus, the overall complexity of GCN+GFS is comparable to that of the original GCN.

5 EXPERIMENTS

To verify the effectiveness of our proposed Graph Feature Selection (GFS) and Topological Feature Informativeness (TFI), we answer the following research questions with experimental evaluations.

RQ1: To what extent does GFS enhance the performance of GNNs?

RQ2: Can GFS universally improve GNN performance without the need for hyperparameter tuning?

RQ3: How does TFI compare to other statistic-based and optimization-based metrics in the context of GFS?

RQ4: Do the GNN-favored and GNN-disfavored features identified by TFI truly align better with GNNs or MLPs, respectively?

5.1 EXPERIMENTAL SETUPS

Data Preparation. The datasets used in our experiments include *Children*, *Computers*, *Fitness*, *History*, and *Photo* from Yan et al. (2023), and *Amazon-Ratings*, *Minesweeper*, *Questions*, *Roman-Empire*, and *Tolokers* from Platonov et al. (2023). These datasets exhibit varying levels of label homophily across different domains. The dataset statistics and descriptions are shown in Appendix C.1. For all datasets, we randomly split the data into training, validation, and test sets in a ratio of 50% : 25% : 25% for 10 runs. Note that the node features in datasets from Yan et al. (2023) are encoded by Pretrained Language Models (PLMs).

Baselines. We implement GFS and compare its performance with 5 baseline GNNs, GCN (Kipf & Welling, 2016), GAT (Veličković et al., 2017), GraphSAGE (SAGE) (Hamilton et al., 2017),

SGC (Wu et al., 2019a) and APPNP (Gasteiger et al., 2018), and 3 SOTA GNNs, Graph Transformer (GT) (Shi et al., 2020), ACM-GCN (Luan et al., 2022a) and FAGCN (Bo et al., 2021). The GFS-augmented GNN is denoted as GNN+GFS throughout this paper. To enhance performance, we incorporate skip connections (He et al., 2016) and layer normalization (Ba et al., 2016) for all the methods, as recommended in Platonov et al. (2023); Luo et al. (2024). The detailed descriptions of these GNNs are introduced in Appendix C.2. Additionally, we compare our proposed TFI with other statistic-based metrics, including h_{GE} (Jin et al., 2022), h_{attr} (Yang et al., 2021b), $h_{sim-cos}$ (Chen et al., 2023), $h_{sim-euc}$ (Chen et al., 2023), and h_{CTF} (Lee et al., 2024). We also evaluate optimization-based metrics such as θ_{Soft} and θ_{Hard} within GFS. Detailed definitions of these statistic-based metrics and optimization-based metrics can be found in Appendix A and Appendix C.4, respectively.

Training. During training, we utilize the Adam optimizer (Kingma & Ba, 2014) to update model parameters. Each model is trained for 1000 epochs, with the epoch demonstrating the best performance on the validation set selected for testing. Model performance is evaluated on node classification tasks, measuring accuracy for multi-class datasets and AUC-ROC for binary-class datasets. The searching space for the ratio r is $\{0.1, 0.2, \dots, 0.9\}$ in GFS³ and $k = 1$ for the number of the hop of neighbors in TFI⁴. See Appendix C.3 for more training details.

5.2 PERFORMANCE (RQ1)

The results and comparisons of the model performance are shown in Table 1, where the performance gap between GNN+GFS and GNN is denoted as Δ . We observe that **(1)** GFS significantly boosts GNN performance on 90%(72/80) cases of the GFS-augmented GNNs, with an average increase of 3.2% in accuracy or AUC-ROC on node classification tasks with various homophily levels. This demonstrate the effectiveness of our proposed method. **(2)** We notice that the improvement of GFS varies by dataset, *e.g.*, in *Children* and *Computers*, GCN+GFS achieves a 5% average performance improvement, while in *Minesweeper* and *Questions*, the improvement is less significant. This may be because most features in *Minesweeper* and *Questions* are already GNN-favored. Nevertheless, GFS remains effective on most datasets. **(3)** We find that GFS demonstrates greater improvements on datasets encoded by Pretrained Language Models (PLMs) (40/40 cases) than those encoded by some traditional methods (32/40 cases), *e.g.*, one-hot, fasttext or statistics-based methods. This suggests that, compared to traditional feature encoding methods, which is widely used in graph learning, **PLMs potentially enable the disentanglement of topology-aware and topology-agnostic information into separate feature dimensions**, further enhancing the effectiveness of GNN+GFS. This is a surprising discovery and to our knowledge, we are the first to reveal this phenomenon. It can help explain why PLMs can assist the learning of graph models (Ye et al., 2024). It would be interesting to analyze each node feature encoded by PLMs in the future, but we will not conduct a deeper discussion in this paper.

5.3 SENSITIVITY TO HYPERPARAMETERS (RQ2)

Some recent GNNs (Li et al., 2022; Liu et al., 2022) introduce more and more hyperparameters, which could be fragile to hyperparameter tuning (Luan et al., 2024c). To investigate the sensitivity of the superiority of GFS over GNNs to ratio r and other model hyperparameters, we compare the performance between GCN and GCN+GFS under varying settings. First, we observe how model performance responds to changes in ratio r , while fixing all other hyperparameters. Figure 4 shows the response of GCN+GFS to r on 4 datasets, where GFS collapses to normal GCN when $r = 1.0$ or MLP when $r = 0.0$, as all features are sent to GNN or MLP, respectively. On *Children*, *Computer*, and *Roman-Empire*, GCN+GFS with $r = 0.1$ to 0.9 consistently outperforms GCN ($r = 1.0$) and MLP ($r = 0.0$), indicating the performance gain obtained from GFS is robust to hyperparameter r . We also observe that although on Tolokers GCN+GFS cannot significantly outperform GCN, sending all the features into GCN ($r = 1.0$) is comparable to sending 40% ($r = 0.4$) to 90% ($r = 0.9$)

³To prevent the behavior of GNN+GFS from closely resembling that of traditional GNNs, we exclude $r = 1.0$ from our experiments. However, in practice, $r = 1.0$ may occur in GNN+GFS when all features are graph-favored, which would make GNN+GFS comparable to GNNs in the worst-case scenario.

⁴In Appendix D.4, we examine the influence of the number of k-hop neighbors on TFI. Our findings indicate that $k = 1$ is sufficient to achieve strong model performance.

Table 1: The performance of GFS on GNN baselines. The improvement is highlighted as **bold** if there is an increase, *i.e.*, $\Delta > 0$, after applying GFS.

Model	Children	Comp.	Fitness	History	Photo	Amazon.	Mines.	Questions	Roman.	Tolokers
GCN	53.88±0.37	83.38±1.78	87.56±0.79	84.26±0.38	84.48±0.65	51.40±0.49	90.01±0.53	76.28±1.18	75.51±0.65	84.19±0.75
GCN+GFS	59.29±0.31	90.23±0.18	93.09±0.13	84.99±0.38	87.31±0.36	53.32±0.81	89.99±0.60	76.50±1.38	83.30±0.57	85.01±0.91
Δ	+5.41	+6.85	+5.53	+0.73	+2.83	+1.92	-0.02	+0.22	+7.79	+0.82
GAT	53.54±0.49	86.52±0.92	88.23±0.91	83.83±0.27	85.67±0.45	51.08±0.60	90.26±0.53	77.64±1.15	84.57±0.80	83.41±0.47
GAT+GFS	57.74±0.35	90.50±0.20	93.20±0.11	84.54±0.38	87.58±0.28	53.75±0.57	90.22±0.64	77.03±1.11	86.17±0.56	84.41±0.77
Δ	+4.20	+3.98	+4.97	+0.71	+1.91	+2.67	-0.04	-0.61	+1.60	+1.00
SAGE	54.68±0.84	86.08±0.50	88.65±1.22	84.06±0.42	85.08±0.64	53.80±0.56	90.74±0.59	74.91±1.06	82.81±0.61	82.77±0.38
SAGE+GFS	59.14±0.33	90.47±0.24	93.63±0.10	84.68±0.33	87.23±0.51	54.17±0.61	90.71±0.62	75.37±1.33	85.47±0.53	83.16±0.73
Δ	+4.46	+4.39	+4.98	+0.62	+2.15	+0.37	-0.03	+0.46	+2.66	+0.39
GT	51.20±0.38	85.63±1.16	87.37±1.38	83.61±0.43	83.65±0.59	51.30±0.73	90.11±0.57	77.57±1.09	84.95±0.54	83.20±0.60
GT+GFS	56.01±0.35	89.97±0.27	92.44±0.11	84.09±0.32	87.41±0.41	52.47±0.54	89.93±0.64	77.70±0.73	86.99±0.45	83.46±0.67
Δ	+4.81	+4.34	+5.07	+0.48	+3.76	+1.17	-0.18	+0.13	+2.04	+0.26
SGC	52.69±0.52	82.50±0.34	84.23±0.31	83.98±0.37	82.79±0.45	49.00±0.42	76.43±1.01	71.78±0.81	69.89±0.51	78.65±1.01
SGC+GFS	55.93±0.37	87.78±0.40	90.29±0.25	84.15±0.23	85.46±0.33	51.43±0.64	88.79±0.66	73.53±1.10	74.00±0.67	82.76±0.84
Δ	+3.24	+5.28	+6.06	+0.17	+2.67	+2.43	+12.36	+1.75	+4.11	+4.11
APPNP	50.63±0.89	83.67±0.90	86.76±1.18	83.37±0.26	82.20±1.41	48.73±0.61	81.61±0.79	75.29±1.06	71.48±0.65	79.82±1.17
APPNP+GFS	56.71±0.36	88.51±0.34	91.22±0.25	84.75±0.33	86.65±0.32	50.76±0.62	83.19±0.97	75.66±1.03	72.35±0.69	83.66±0.65
Δ	+6.08	+4.84	+4.46	+1.38	+4.45	+2.03	+1.58	+0.37	+0.87	+3.84
ACMGCN	54.60±0.50	85.94±0.72	89.10±0.98	84.22±0.34	84.99±0.34	51.91±0.39	90.59±0.58	76.66±1.27	85.27±0.57	83.61±0.83
ACMGCN+GFS	59.04±0.37	89.59±0.19	93.44±0.07	84.70±0.30	86.61±0.42	52.81±0.75	90.45±0.59	75.99±1.27	87.03±0.57	83.45±1.03
Δ	+4.44	+3.65	+4.34	+0.48	+1.62	+0.90	-0.14	-0.67	+1.76	-0.16
FAGCN	50.43±0.86	79.92±0.99	83.10±0.45	82.04±0.62	80.67±0.77	46.08±0.52	78.22±2.86	58.60±2.08	62.02±2.98	73.07±0.70
FAGCN+GFS	56.17±0.38	87.72±0.49	89.66±0.35	84.32±0.36	85.54±0.37	50.72±0.82	88.12±1.32	71.94±2.03	72.05±1.45	82.82±1.28
Δ	+5.74	+7.80	+6.56	+2.28	+4.87	+4.64	+9.90	+13.34	+10.03	+9.75

features with the highest TFI in GCN+GFS. These results highlight the necessity of GFS, as neither $r = 1.0$ (all features to GCN) nor $r = 0.0$ (all features to MLP) yields optimal results on most datasets, which reduces the need for convoluting all the features.

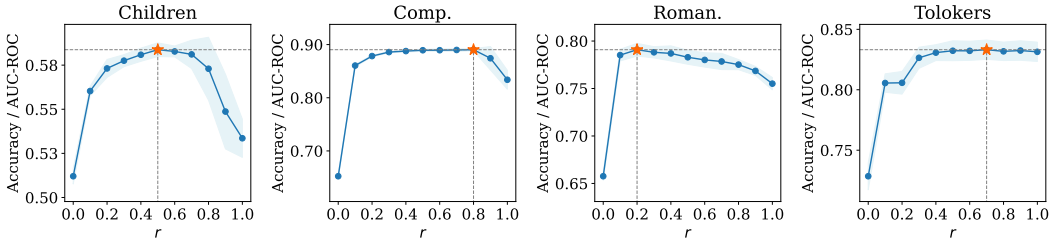


Figure 4: The impact of ratio r to the performance of GCN+GFS is examined, where r features are sent to MLP and $1 - r$ features are sent to GCN. The point representing the best performance is highlighted as \star .

Second, we analyze how other hyperparameters affect GFS performance. Figure 5 shows how GCN, MLP, and GCN+GFS respond to the changes in the number of layers, dimension of hidden embeddings, learning rate, weight decay, and dropout rate on *Computers* (homophilic graph) and *Amazon-Ratings* (heterophilic graph). Results indicate that GCN+GFS consistently outperforms GCN and MLP across various hyperparameter values. This property allows GFS to be easily integrated into other GNNs without much hyperparameter tuning. Please refer to Appendix D.2 for more results on the sensitivity of GFS to hyperparameters on the other datasets.

5.4 EFFECTIVENESS OF TFI (RQ3)

We show the superiority of TFI by comparing GCN+GFS with other metric-based feature selection methods, *e.g.*, statistic-based metrics h_{GE} Jin et al. (2022), h_{attr} Yang et al. (2021a), $h_{sim-cos}$, $h_{sim-euc}$ Chen et al. (2023), and h_{CTF} Lee et al. (2024) and optimization-based methods *e.g.*, θ_{Soft} and θ_{Hard} , where feature selection process is learned in an end-to-end manner. All methods follow the same hyperparameter tuning as in GFS. Table 2 shows the performance of different metrics in feature selection for GCN, where TFI achieves the best performance in average rank across 10 datasets. This is reasonable because other statistic-based metrics suffer from explaining “good heterophily” issue and TFI overcomes the issue by the measurement of mutual information Platonov et al. (2024). Besides, the optimization-based metrics underperform TFI, indicating the feature se-

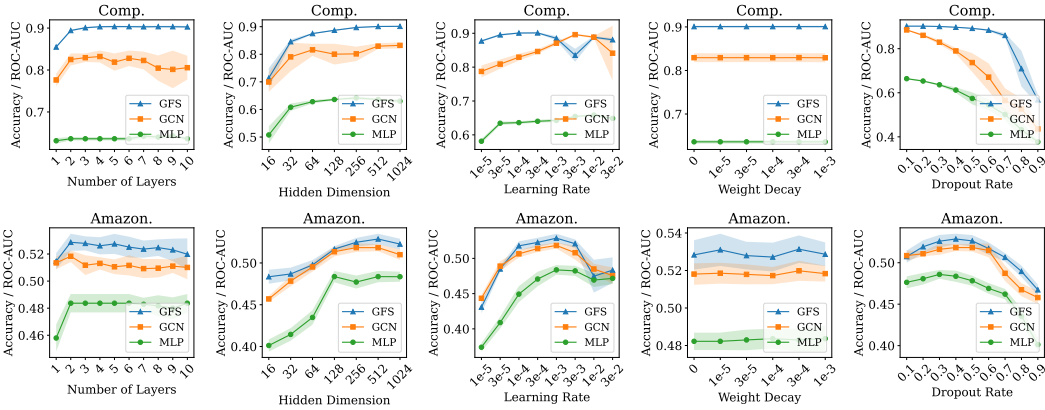


Figure 5: Response of GCN+GFS, GCN, and MLP to 5 hyperparameters on Computers and Amazon-Ratings.

lection cannot be effectively handled automatically during the optimization process of GNNs. In addition, we find that even for the metrics that are inferior to TFI, e.g., h_{attr} , $h_{sim-euc}$ and h_{CTF} , applying them within our GFS framework can still improve the performance of baseline GCN, indicating the necessity of feature selection in GNNs.

Table 2: The performance of feature selection on feature homophily metrics and optimization-based methods.

Metrics	Children	Comp.	Fitness	History	Photo	Amazon.	Mines.	Questions	Roman.	Tolokers	Avg. Rank
TFI	59.29±0.31	90.23±0.18	93.09±0.13	84.99±0.38	87.11±0.42	53.32±0.81	89.99±0.60	76.50±1.38	83.30±0.57	85.01±0.91	1.40
h_{GE}	55.00±0.25	83.72±1.32	87.06±0.58	83.88±0.26	83.36±0.94	51.71±0.53	89.75±0.68	75.73±1.53	79.11±0.48	83.31±0.77	6.70
h_{attr}	55.15±0.32	84.62±0.61	87.88±0.53	84.22±0.25	83.22±0.52	51.46±0.70	90.18±0.70	76.40±1.39	78.90±0.58	84.04±0.82	4.70
$h_{sim-eos}$	55.15±0.51	84.11±0.84	87.09±0.98	84.07±0.31	83.38±1.01	51.68±0.39	89.87±0.53	75.88±1.07	78.98±0.66	83.69±0.82	5.95
$h_{sim-euc}$	56.32±0.26	89.08±0.20	87.52±1.04	85.00±0.38	86.71±0.30	51.35±0.49	90.19±0.69	76.51±1.17	78.96±0.73	84.03±0.83	3.35
h_{CTF}	55.04±0.51	84.80±0.87	88.69±2.25	84.32±0.30	83.46±0.85	51.76±0.57	89.97±0.68	76.40±1.37	78.70±0.38	83.38±0.89	4.55
Soft	57.04±1.37	85.35±3.53	89.54±1.32	84.47±0.92	84.83±3.28	51.70±0.62	89.93±0.60	75.94±1.28	79.20±0.46	84.03±0.84	3.50
Hard	45.28±0.79	66.92±4.70	69.48±4.14	80.98±0.70	72.09±3.72	42.77±0.57	86.62±2.25	75.56±1.29	76.96±0.61	79.13±0.94	8.90
None	53.36±1.08	83.38±1.78	87.56±0.79	84.13±0.29	84.00±0.72	51.40±0.49	89.93±0.52	76.24±1.48	75.51±0.65	84.19±0.75	5.95

Since TFI is not an unsupervised measurement, we investigate how the percentage of supervision in TFI (percentage of node labels used to calculate TFI in Eq. (5)) influences the model performance of GCN+GFS. As shown in Figure 6, as the supervision percentage increases, the model performance first increases and then stabilizes after 30%. This indicates that 30% of the label supervision achieves similar results as full labels in most datasets and it highlights the effectiveness of TFI in sparse label scenarios. Compared to some other methods (Zheng et al., 2024b; Li et al., 2023b) that require pseudo labels during training, TFI requires less preprocessing in semi-supervised node classification settings. Even with only 10% supervision, TFI can still enhance GCN+GFS performance on most datasets compared to the original GCN. Please refer to Appendix D.3 for more results on the influence of the supervision percentage in TFI on GFS performance.

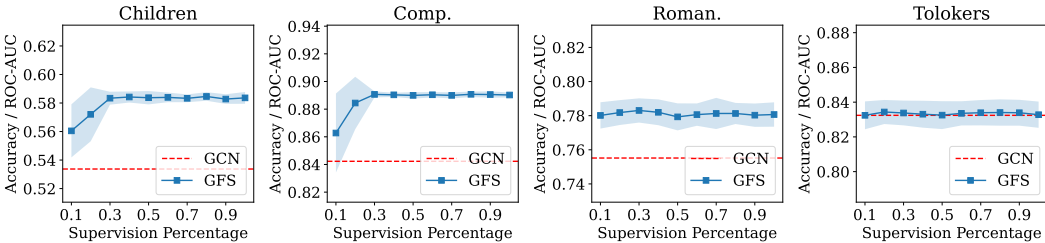


Figure 6: Influence of the percentage of the supervision in TFI on the model performance of GCN+GFS.

Based on TFI, we extend the feature selection from the raw node features to node embeddings, which may also be GNN-favored or GNN-disfavored. Specifically, we train a GCN or MLP on the

training set and then get the node embeddings from the last layer. After that, we train GCN+GFS on these node embeddings following the same process as on the original node features. As shown in Figure 7, applying GCN+GFS on either the original node features, \mathbf{X} , or pretrained node embeddings, $\text{MLP}(\mathbf{X})$ and $\text{GCN}(\mathbf{X}, \mathbf{A})$, improves GCN performance on most datasets. Furthermore, for some datasets, such as Computers, Questions, and Amazon-ratings, the performance of GCN+GFS could be further improved using pretrained node embeddings compared with original node features. Additionally, it would be interesting to explore the impact of graph feature selection on dynamically updated node embeddings in future research.

5.5 GNN-FAVORED AND GNN-DISFAVORED FEATURES (RQ4)

To validate whether features selected by a high TFI are truly GNN-favored, we swapped features by feeding GNN-favored features into MLP and GNN-disfavored features into GNN. As shown in Figure 8, the performance of GCN+GFS drops in all datasets after swapping GNN-favored and GNN-disfavored features. Especially in some datasets, such as Minesweeper, there is a 40% drop in performance. These results show that TFI reliably identifies GNN-favored and GNN-disfavored features.

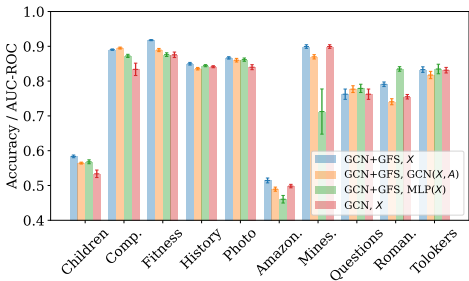


Figure 7: GCN+GFS on node features \mathbf{X} and pretrained node embeddings $\text{GCN}(\mathbf{X}, \mathbf{A})$ and $\text{MLP}(\mathbf{X})$.

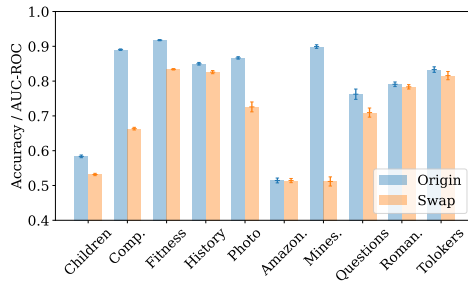


Figure 8: Performance drop of GCN+GFS by swapping GNN-favored and GNN-disfavored features.

6 CONCLUSION AND FUTURE WORKS

In this paper, we study feature selection to enhance GNN performance by identifying GNN-favored and GNN-disfavored features. To answer whether each feature in graphs is GNN-favored or not, previous feature homophily metrics suffer from “good heterophily”. To address this issue, we introduce Topological Feature Informativeness (TFI), which measures the mutual information between aggregated node features and labels. This metric effectively quantifies the performance gap between GNNs and Multi-Layer Perceptrons (MLPs), as supported by our empirical observations and theoretical analyses. We then propose a simple yet effective method, Graph Feature Selection (GFS), to incorporate TFI to improve the GNN performance. Our extensive experiments demonstrate that applying GFS to 8 GNN architectures across 10 datasets yields a significant performance boost in 90% (72 out of 80) of the cases, with an average increase of 3.2% in accuracy or AUC-ROC on node classification tasks. We also show that the performance gains from GFS are robust to hyperparameter tuning, indicating its potential as a universal method for enhancing various types of GNNs.

Admittedly, the features selected by TFI introduce a new hyperparameter, ratio r , in GFS. Although GFS improves GNNs performance across a large range of r , the best performance point remains unknown due to the high complexity of the optimization process in GNNs and MLP. Therefore, it is interesting to explore the auto-selection of ratio r in the future. Furthermore, since TFI is a supervised, statistic-based metric and other types of metrics may also enhance GNN performance under GFS, it would be valuable to investigate more types of metrics, both supervised and unsupervised, for feature selection in graphs with GNNs in the future.

REFERENCES

- 540
541
542 Sami Abu-El-Haija, Bryan Perozzi, Amol Kapoor, Nazanin Alipourfard, Kristina Lerman, Hrayr
543 Harutyunyan, Greg Ver Steeg, and Aram Galstyan. Mixhop: Higher-order graph convolutional
544 architectures via sparsified neighborhood mixing. In *international conference on machine learn-*
545 *ing*, pp. 21–29. PMLR, 2019.
- 546 Jason Ansel, Edward Yang, Horace He, Natalia Gimelshein, and Animesh et al. Jain. PyTorch
547 2: Faster Machine Learning Through Dynamic Python Bytecode Transformation and Graph
548 Compilation. In *29th ACM International Conference on Architectural Support for Program-*
549 *ming Languages and Operating Systems, Volume 2 (ASPLOS '24)*. ACM, April 2024. doi:
550 10.1145/3620665.3640366. URL <https://pytorch.org/assets/pytorch2-2.pdf>.
- 551 AK Awasthi, Arun Kumar Garov, Minakshi Sharma, and Mrigank Sinha. Gnn model based on
552 node classification forecasting in social network. In *2023 International Conference on Artificial*
553 *Intelligence and Smart Communication (AISC)*, pp. 1039–1043. IEEE, 2023.
- 554 Jimmy Lei Ba, Jamie Ryan Kiros, and Geoffrey E Hinton. Layer normalization. *arXiv preprint*
555 *arXiv:1607.06450*, 2016.
- 556 Deyu Bo, Xiao Wang, Chuan Shi, and Huawei Shen. Beyond low-frequency information in graph
557 convolutional networks. In *Proceedings of the AAAI conference on artificial intelligence*, vol-
558 *ume 35*, pp. 3950–3957, 2021.
- 559 Yuhan Chen, Yihong Luo, Jing Tang, Liang Yang, Siya Qiu, Chuan Wang, and Xiaochun Cao.
560 Lsgnn: towards general graph neural network in node classification by local similarity. *arXiv*
561 *preprint arXiv:2305.04225*, 2023.
- 562 John C Davis, Robert J Sampson, et al. *Statistics and data analysis in geology*, volume 646. Wiley
563 New York, 1986.
- 564 Ben Finkelshtein, Xingyue Huang, Michael Bronstein, and Ismail Ilkan Ceylan. Cooperative graph
565 neural networks. *arXiv preprint arXiv:2310.01267*, 2023.
- 566 Johannes Gasteiger, Aleksandar Bojchevski, and Stephan Günnemann. Predict then propagate:
567 Graph neural networks meet personalized pagerank. *arXiv preprint arXiv:1810.05997*, 2018.
- 568 Sebastien Gerchinovitz, Pierre Ménard, and Gilles Stoltz. Fano’s inequality for random variables.
569 2020.
- 570 Edouard Grave, Piotr Bojanowski, Prakhar Gupta, Armand Joulin, and Tomas Mikolov. Learning
571 word vectors for 157 languages. In *Proceedings of the Eleventh International Conference on Lan-*
572 *guage Resources and Evaluation (LREC 2018)*, Miyazaki, Japan, May 2018. European Language
573 Resources Association (ELRA). URL <https://aclanthology.org/L18-1550>.
- 574 Will Hamilton, Zhitao Ying, and Jure Leskovec. Inductive representation learning on large graphs.
575 *Advances in neural information processing systems*, 30, 2017.
- 576 Haoyu Han, Juanhui Li, Wei Huang, Xianfeng Tang, Hanqing Lu, Chen Luo, Hui Liu, and Jiliang
577 Tang. Node-wise filtering in graph neural networks: A mixture of experts approach. *arXiv*
578 *preprint arXiv:2406.03464*, 2024.
- 579 Satoshi Hara and Takanori Maehara. Enumerate lasso solutions for feature selection. In *Proceedings*
580 *of the AAAI Conference on Artificial Intelligence*, volume 31, 2017.
- 581 Kaiming He, Xiangyu Zhang, Shaoqing Ren, and Jian Sun. Deep residual learning for image recog-
582 *nition*. In *Proceedings of the IEEE conference on computer vision and pattern recognition*, pp.
583 770–778, 2016.
- 584 Xiaofei He, Deng Cai, and Partha Niyogi. Laplacian score for feature selection. *Advances in neural*
585 *information processing systems*, 18, 2005.
- 586 Matthew Honnibal, Ines Montani, Sofie Van Landeghem, and Adriane Boyd. spaCy: Industrial-
587 *strength Natural Language Processing in Python*. 2020. doi: 10.5281/zenodo.1212303.

- 594 Chenqing Hua, Sitao Luan, Minkai Xu, Zhitao Ying, Jie Fu, Stefano Ermon, and Doina Precup.
595 Mudiff: Unified diffusion for complete molecule generation. In *Learning on Graphs Conference*,
596 pp. 33–1. PMLR, 2024.
- 597 Eric Jang, Shixiang Gu, and Ben Poole. Categorical reparameterization with gumbel-softmax. In *5th*
598 *International Conference on Learning Representations, ICLR 2017, Toulon, France, April 24-26,*
599 *2017, Conference Track Proceedings*. OpenReview.net, 2017. URL <https://openreview.net/forum?id=rkE3y85ee>.
- 602 Di Jin, Rui Wang, Meng Ge, Dongxiao He, Xiang Li, Wei Lin, and Weixiong Zhang. Raw-gnn:
603 Random walk aggregation based graph neural network. *arXiv preprint arXiv:2206.13953*, 2022.
- 604 Chuanze Kang, Han Zhang, Zhuo Liu, Shenwei Huang, and Yanbin Yin. Lr-gnn: A graph neural
605 network based on link representation for predicting molecular associations. *Briefings in Bioinform-*
606 *atics*, 23(1):bbab513, 2022.
- 608 Kazi Zainab Khanam, Gautam Srivastava, and Vijay Mago. The homophily principle in social
609 network analysis: A survey. *Multimedia Tools and Applications*, 82(6):8811–8854, 2023.
- 610 Seyoung Kim and Eric P Xing. Statistical estimation of correlated genome associations to a quanti-
611 tative trait network. *PLoS genetics*, 5(8):e1000587, 2009.
- 613 Diederik P Kingma and Jimmy Ba. Adam: A method for stochastic optimization. *arXiv preprint*
614 *arXiv:1412.6980*, 2014.
- 615 Thomas N Kipf and Max Welling. Semi-supervised classification with graph convolutional net-
616 works. *arXiv preprint arXiv:1609.02907*, 2016.
- 618 Alexander Kraskov, Harald Stögbauer, and Peter Grassberger. Estimating mutual information. *Phys-*
619 *ical Review E—Statistical, Nonlinear, and Soft Matter Physics*, 69(6):066138, 2004.
- 620 Soo Yong Lee, Sunwoo Kim, Fanchen Bu, Jaemin Yoo, Jiliang Tang, and Kijung Shin. Feature
621 distribution on graph topology mediates the effect of graph convolution: Homophily perspective.
622 *International Conference on Machine Learning*, 2024.
- 624 Jure Leskovec and Andrej Krevl. SNAP Datasets: Stanford large network dataset collection. [http://](http://snap.stanford.edu/data)
625 snap.stanford.edu/data, June 2014.
- 626 David D Lewis. Feature selection and feature extraction for text categorization. In *Speech and*
627 *Natural Language: Proceedings of a Workshop Held at Harriman, New York, February 23-26,*
628 *1992*, 1992.
- 630 Jundong Li, Kewei Cheng, Suhang Wang, Fred Morstatter, Robert P Trevino, Jiliang Tang, and Huan
631 Liu. Feature selection: A data perspective. *ACM computing surveys (CSUR)*, 50(6):1–45, 2017.
- 632 Xiang Li, Renyu Zhu, Yao Cheng, Caihua Shan, Siqiang Luo, Dongsheng Li, and Weining Qian.
633 Finding global homophily in graph neural networks when meeting heterophily. In *International*
634 *Conference on Machine Learning*, pp. 13242–13256. PMLR, 2022.
- 636 Xiao Li, Li Sun, Mengjie Ling, and Yan Peng. A survey of graph neural network based recommen-
637 dation in social networks. *Neurocomputing*, 549:126441, 2023a.
- 638 Yayong Li, Jie Yin, and Ling Chen. Informative pseudo-labeling for graph neural networks with
639 few labels. *Data Mining and Knowledge Discovery*, 37(1):228–254, 2023b.
- 641 Daniil Likhobaba, Nikita Pavlichenko, and Dmitry Ustalov. Toloker Graph: Interaction of Crowd
642 Annotators, 2023. URL <https://github.com/Toloka/TolokerGraph>.
- 643 Derek Lim, Xiuyu Li, Felix Hohne, and Ser-Nam Lim. New benchmarks for learning on non-
644 homophilous graphs. *arXiv preprint arXiv:2104.01404*, 2021.
- 646 Huan Liu and Rudy Setiono. Chi2: Feature selection and discretization of numeric attributes. In
647 *Proceedings of 7th IEEE international conference on tools with artificial intelligence*, pp. 388–
391. Ieee, 1995.

- 648 Nian Liu, Xiao Wang, Lingfei Wu, Yu Chen, Xiaojie Guo, and Chuan Shi. Compact Graph Structure
649 Learning via Mutual Information Compression, January 2022. URL [http://arxiv.org/](http://arxiv.org/abs/2201.05540)
650 [abs/2201.05540](http://arxiv.org/abs/2201.05540). arXiv:2201.05540 [cs].
- 651 Qincheng Lu, Sitao Luan, and Xiao-Wen Chang. Gcepnet: Graph convolution-enhanced expectation
652 propagation for massive mimo detection. In *IEEE GLOBECOM 2024 Conference Proceedings*,
653 2024a.
- 654 Qincheng Lu, Jiaqi Zhu, Sitao Luan, and Xiao-Wen Chang. Flexible diffusion scopes with parameterized
655 laplacian for heterophilic graph learning. *arXiv preprint arXiv:2409.09888*, 2024b.
- 656 Sitao Luan, Mingde Zhao, Xiao-Wen Chang, and Doina Precup. Break the ceiling: Stronger multi-
657 scale deep graph convolutional networks. *Advances in neural information processing systems*, 32,
658 2019.
- 659 Sitao Luan, Chenqing Hua, Qincheng Lu, Jiaqi Zhu, Mingde Zhao, Shuyuan Zhang, Xiao-Wen
660 Chang, and Doina Precup. Revisiting heterophily for graph neural networks. *Advances in neural
661 information processing systems*, 35:1362–1375, 2022a.
- 662 Sitao Luan, Mingde Zhao, Chenqing Hua, Xiao-Wen Chang, and Doina Precup. Complete the
663 missing half: Augmenting aggregation filtering with diversification for graph convolutional neural
664 networks. *arXiv preprint arXiv:2212.10822*, 2022b.
- 665 Sitao Luan, Chenqing Hua, Qincheng Lu, Liheng Ma, Lirong Wu, Xinyu Wang, Minkai Xu,
666 Xiao-Wen Chang, Doina Precup, Rex Ying, et al. The heterophilic graph learning hand-
667 book: Benchmarks, models, theoretical analysis, applications and challenges. *arXiv preprint
668 arXiv:2407.09618*, 2024a.
- 669 Sitao Luan, Chenqing Hua, Minkai Xu, Qincheng Lu, Jiaqi Zhu, Xiao-Wen Chang, Jie Fu, Jure
670 Leskovec, and Doina Precup. When do graph neural networks help with node classification?
671 investigating the homophily principle on node distinguishability. *Advances in Neural Information
672 Processing Systems*, 36, 2024b.
- 673 Sitao Luan, Qincheng Lu, Chenqing Hua, Xinyu Wang, Jiaqi Zhu, Xiao-Wen Chang, Guy Wolf,
674 and Jian Tang. Are heterophily-specific gnns and homophily metrics really effective? evaluation
675 pitfalls and new benchmarks. *arXiv preprint arXiv:2409.05755*, 2024c.
- 676 Yuankai Luo, Lei Shi, and Xiao-Ming Wu. Classic gnns are strong baselines: Reassessing gnns for
677 node classification. *arXiv preprint arXiv:2406.08993*, 2024.
- 678 Yao Ma, Xiaorui Liu, Neil Shah, and Jiliang Tang. Is homophily a necessity for graph neural
679 networks? *arXiv preprint arXiv:2106.06134*, 2021.
- 680 Miller McPherson, Lynn Smith-Lovin, and James M Cook. Birds of a feather: Homophily in social
681 networks. *Annual review of sociology*, 27(1):415–444, 2001.
- 682 Hongbin Pei, Bingzhe Wei, Kevin Chen-Chuan Chang, Yu Lei, and Bo Yang. Geom-gcn: Geometric
683 graph convolutional networks. *arXiv preprint arXiv:2002.05287*, 2020a.
- 684 Hongbin Pei, Bingzhe Wei, Kevin Chen-Chuan Chang, Yu Lei, and Bo Yang. Geom-gcn: Geometric
685 graph convolutional networks. *arXiv preprint arXiv:2002.05287*, 2020b.
- 686 Oleg Platonov, Denis Kuznedelev, Michael Diskin, Artem Babenko, and Liudmila Prokhorenkova.
687 A critical look at the evaluation of gnns under heterophily: Are we really making progress? *arXiv
688 preprint arXiv:2302.11640*, 2023.
- 689 Oleg Platonov, Denis Kuznedelev, Artem Babenko, and Liudmila Prokhorenkova. Characterizing
690 graph datasets for node classification: Homophily-heterophily dichotomy and beyond. *Advances
691 in Neural Information Processing Systems*, 36, 2024.
- 692 Fazlollah M Reza. *An introduction to information theory*. Courier Corporation, 1994.
- 693 Brian C Ross. Mutual information between discrete and continuous data sets. *PloS one*, 9(2):
694 e87357, 2014.

- 702 Yunsheng Shi, Zhengjie Huang, Shikun Feng, Hui Zhong, Wenjin Wang, and Yu Sun. Masked label
703 prediction: Unified message passing model for semi-supervised classification. *arXiv preprint*
704 *arXiv:2009.03509*, 2020.
- 705
706 Petar Velicković, Guillem Cucurull, Arantxa Casanova, Adriana Romero, Pietro Lio, and Yoshua
707 Bengio. Graph attention networks. *arXiv preprint arXiv:1710.10903*, 2017.
- 708
709 Junfu Wang, Yuanfang Guo, Liang Yang, and Yunhong Wang. Understanding heterophily for graph
710 neural networks. *arXiv preprint arXiv:2401.09125*, 2024a.
- 711
712 Kun Wang, Guohao Li, Shilong Wang, Guibin Zhang, Kai Wang, Yang You, Junfeng Fang, Xiao-
713 jiang Peng, Yuxuan Liang, and Yang Wang. The snowflake hypothesis: Training and powering
714 gnn with one node one receptive field. In *Proceedings of the 30th ACM SIGKDD Conference on*
Knowledge Discovery and Data Mining, pp. 3152–3163, 2024b.
- 715
716 Minjie Wang, Da Zheng, Zihao Ye, Quan Gan, Mufei Li, Xiang Song, Jinjing Zhou, Chao Ma,
717 Lingfan Yu, Yu Gai, Tianjun Xiao, Tong He, George Karypis, Jinyang Li, and Zheng Zhang.
718 Deep graph library: A graph-centric, highly-performant package for graph neural networks. *arXiv*
preprint arXiv:1909.01315, 2019.
- 719
720 Shilong Wang, Hao Wu, Yifan Duan, Guibin Zhang, Guohao Li, Yuxuan Liang, Shirui Pan, Kun
721 Wang, and Yang Wang. All nodes are created not equal: Node-specific layer aggregation and
722 filtration for gnn. *arXiv preprint arXiv:2405.07892*, 2024c.
- 723
724 Felix Wu, Amauri Souza, Tianyi Zhang, Christopher Fifty, Tao Yu, and Kilian Weinberger. Sim-
725 plifying graph convolutional networks. In *International conference on machine learning*, pp.
726 6861–6871. PMLR, 2019a.
- 727
728 Shiwen Wu, Fei Sun, Wentao Zhang, Xu Xie, and Bin Cui. Graph neural networks in recommender
729 systems: a survey. *ACM Computing Surveys*, 55(5):1–37, 2022.
- 730
731 Shu Wu, Yuyuan Tang, Yanqiao Zhu, Liang Wang, Xing Xie, and Tieniu Tan. Session-based rec-
732 ommendation with graph neural networks. In *Proceedings of the AAAI conference on artificial*
intelligence, volume 33, pp. 346–353, 2019b.
- 733
734 Hao Yan, Chaozhuo Li, Ruosong Long, Chao Yan, Jianan Zhao, Wenwen Zhuang, Jun Yin, Peiyan
735 Zhang, Weihao Han, Hao Sun, et al. A comprehensive study on text-attributed graphs: Bench-
736 marking and rethinking. *Advances in Neural Information Processing Systems*, 36:17238–17264,
2023.
- 737
738 Liang Yang, Mengzhe Li, Liyang Liu, Chuan Wang, Xiaochun Cao, Yuanfang Guo, et al. Diverse
739 message passing for attribute with heterophily. *Advances in Neural Information Processing Sys-*
tems, 34:4751–4763, 2021a.
- 740
741 Liang Yang, Mengzhe Li, Liyang Liu, Chuan Wang, Xiaochun Cao, Yuanfang Guo, et al. Diverse
742 message passing for attribute with heterophily. *Advances in Neural Information Processing Sys-*
tems, 34:4751–4763, 2021b.
- 743
744 Jieping Ye and Jun Liu. Sparse methods for biomedical data. *ACM Sigkdd Explorations Newsletter*,
745 14(1):4–15, 2012.
- 746
747 Ruosong Ye, Caiqi Zhang, Runhui Wang, Shuyuan Xu, and Yongfeng Zhang. Language is all a
748 graph needs. In *Findings of the Association for Computational Linguistics: EACL 2024*, pp.
749 1955–1973, 2024.
- 750
751 Xiao-Meng Zhang, Li Liang, Lin Liu, and Ming-Jing Tang. Graph neural networks and their current
752 applications in bioinformatics. *Frontiers in genetics*, 12:690049, 2021.
- 753
754 Tianxiang Zhao, Xiang Zhang, and Suhang Wang. Disambiguated node classification with graph
755 neural networks. In *Proceedings of the ACM on Web Conference 2024*, pp. 914–923, 2024.
- 756
757 Zheng Zhao and Huan Liu. Spectral feature selection for supervised and unsupervised learning. In
Proceedings of the 24th international conference on Machine learning, pp. 1151–1157, 2007.

756 Yilun Zheng, Sitao Luan, and Lihui Chen. What is missing in homophily? disentangling graph
757 homophily for graph neural networks. *arXiv preprint arXiv:2406.18854*, 2024a.
758

759 Yilun Zheng, Jiahao Xu, and Lihui Chen. Learn from heterophily: Heterophilous information-
760 enhanced graph neural network. *arXiv preprint arXiv:2403.17351*, 2024b.

761 Ji Zhu, Saharon Rosset, Robert Tibshirani, and Trevor Hastie. 1-norm support vector machines.
762 *Advances in neural information processing systems*, 16, 2003.
763

764 Jiong Zhu, Yujun Yan, Lingxiao Zhao, Mark Heimann, Leman Akoglu, and Danai Koutra. Beyond
765 homophily in graph neural networks: Current limitations and effective designs. *Advances in*
766 *Neural Information Processing Systems*, 33, 2020a.

767 Jiong Zhu, Yujun Yan, Lingxiao Zhao, Mark Heimann, Leman Akoglu, and Danai Koutra. Beyond
768 homophily in graph neural networks: Current limitations and effective designs. *Advances in*
769 *neural information processing systems*, 33:7793–7804, 2020b.
770
771
772
773
774
775
776
777
778
779
780
781
782
783
784
785
786
787
788
789
790
791
792
793
794
795
796
797
798
799
800
801
802
803
804
805
806
807
808
809

A RELATED WORK

The proposed Graph Feature Selection (GFS) in this paper mainly relates with feature selection and GNNs efficacy. Thus, in this section, we first introduce feature selection methods on non-GNNs models and GNNs. Then, we introduce the studies on the effectiveness of GNNs from a graph level, node level, or feature level.

Feature Selection. Feature selection is crucial for improving model performance, preventing overfitting, and reducing computational complexity (Li et al., 2017). To preserve data similarity, Laplacian Score (He et al., 2005) and SPEC (Zhao & Liu, 2007) are proposed to select features that best preserve the data manifold structure. To maximize the correlation between feature and class labels, MIM (Lewis, 1992) is proposed based on information theory. To minimize the fitting errors in classification tasks, Hara & Maehara (2017); Zhu et al. (2003) propose to select features with larger weights in models with l_1 -norm regularization. To reduce feature redundancy, T-Score (Davis et al., 1986) and Chi-Square Score (Liu & Setiono, 1995) are proposed to access whether features could distinguish different classes. All of the aforementioned methods only consider data in Euclidean space, which cannot be applied for non-Euclidean data, such as graph-structured data. To address this, Ye & Liu (2012); Kim & Xing (2009) use a Graph Lasso regularizer to select features consistent across connected nodes.

While effective in traditional machine learning, these methods do not identify GNN-favored or GNN-disfavored features, as discussed in this paper. Our approach does not simply discard GNN-disfavored features; instead, it strategically utilizes them with a non-GNN model, driven by the principle of aligning the right features with the right model.

Graph Homophily. Even if traditional GNNs (Kipf & Welling, 2016; Velicković et al., 2017) are believed to perform well on graph-related tasks, the performance of GNNs could be inferior than non-GNNs models in some graphs. Therefore, metrics of graph homophily, such as edge homophily (Zhu et al., 2020a), node homophily (Pei et al., 2020b), and class homophily (Lim et al., 2021), are proposed to determine when GNNs perform well. The definitions of these homophily metrics are given as:

$$h_{\text{edge}}(\mathcal{G}, \mathbf{Y}) = \frac{|\{e_{uv} | e_{uv} \in \mathcal{E}, Y_u = Y_v\}|}{|\mathcal{E}|}, \quad h_{\text{node}}(\mathcal{G}, \mathbf{Y}) = \frac{1}{|\mathcal{V}|} \sum_{v \in \mathcal{V}} \frac{|\{u | u \in \mathcal{N}_v, Y_u = Y_v\}|}{|\mathcal{N}_v|} \quad (10)$$

$$h_{\text{class}}(\mathcal{G}, \mathbf{Y}) = \frac{1}{C-1} \sum_{c=1}^C \left[\frac{\sum_{u \in \mathcal{V}, Y_u=c} |\{v | v \in \mathcal{N}_u, Y_u = Y_v\}|}{\sum_{u \in \{u | Y_u=c\}} d_u} - \frac{N_c}{N} \right]_+ \quad (11)$$

$$h_{\text{adj}}(\mathcal{G}, \mathbf{Y}) = \frac{h_{\text{edge}}(\mathcal{G}, \mathbf{Y}) - \sum_{c=1}^C \frac{D_c^2}{(2|\mathcal{E}|)^2}}{1 - \sum_{c=1}^C \frac{D_c^2}{(2|\mathcal{E}|)^2}} \quad (12)$$

Generally, these metrics measure the label consistency along the graph topology using an indicator function to determine if the connected nodes share the same labels. However, these metrics suffering from the "good heterophily" (Ma et al., 2021), leading to a misalignment with GNNs performance. Therefore, new metrics, such as label informativeness (Platonov et al., 2024), aggregation homophily (Luan et al., 2022a), and classifier-based homophily (Luan et al., 2024b) are proposed to mitigate this deficiency. Nevertheless, all these metrics neglect the feature aspect in graphs, which also constitute an important role in GNNs performance (Zheng et al., 2024a). Therefore, some feature homophily metrics, such as generalized edge homophily (Jin et al., 2022) is proposed to measure the feature consistency across the graph topology:

$$h_{GE}(\mathcal{G}, \mathbf{X}) = \frac{1}{|\mathcal{E}|} \sum_{e_{uv} \in \mathcal{E}} \frac{\mathbf{X}_u \mathbf{X}_v}{\|\mathbf{X}_u\| \|\mathbf{X}_v\|} \quad (13)$$

864 Similarly, local similarity (Chen et al., 2023) is proposed to measure feature homophily at the node
865 level by cosine similarity or Euclidean similarity:

$$866 \quad h_{LS-cos}(\mathcal{G}, \mathbf{X}) = \frac{1}{|\mathcal{V}|} \sum_{u \in \mathcal{V}} \frac{1}{d_u} \sum_{v \in \mathcal{N}_u} \frac{\mathbf{X}_u \mathbf{X}_v}{\|\mathbf{X}_u\| \|\mathbf{X}_v\|}$$

$$867 \quad h_{LS-euc}(\mathcal{G}, \mathbf{X}) = \frac{1}{|\mathcal{V}|} \sum_{u \in \mathcal{V}} \frac{1}{d_u} \sum_{v \in \mathcal{N}_u} (-\|\mathbf{X}_u - \mathbf{X}_v\|_2)$$
(14)

871 Attribute homophily (Yang et al., 2021b) also consider the feature homophily but with a different
872 normalization on each feature:

$$873 \quad h_{attr,m}(\mathcal{G}, \mathbf{X}_{:,m}) = \frac{1}{\sum_{u \in \mathcal{V}} X_{u,m}} \sum_{u \in \mathcal{V}} \left(X_{u,m} \frac{\sum_{v \in \mathcal{N}_u} X_{v,m}}{d_u} \right)$$

$$874 \quad h_{attr}(\mathcal{G}, \mathbf{X}) = \sum_{m=1}^M h_{attr,m}(\mathcal{G}, \mathbf{X}_{:,m})$$
(15)

879 Class-controlled feature homophily (Lee et al., 2024) examines the relationship between graph
880 topology and feature dependence by analyzing the difference in expected distances between a node
881 and its neighbors compared to random nodes, defined as follows:

$$882 \quad h_{CF}(\mathcal{G}, \mathbf{X}, \mathbf{Y}) = \frac{1}{|\mathcal{V}|} \sum_{u \in \mathcal{V}} \frac{1}{d_u} \sum_{v \in \mathcal{N}_u} \left(d(v, \mathcal{V} \setminus \{u\}) - d(v, \{u\}) \right)$$

$$883 \quad d(u, \mathcal{V}') = \frac{1}{|\mathcal{V}'|} \sum_{v \in \mathcal{V}'} \left\| (\mathbf{X}_u | \mathbf{Y}) - (\mathbf{X}_v | \mathbf{Y}) \right\|$$

$$884 \quad \mathbf{X}_u | \mathbf{Y} = \mathbf{X}_u - \left(\frac{\sum_{Y_u=Y_v} \mathbf{X}_v}{|\{v | Y_u=Y_v, v \in \mathcal{V}\}|} \right)$$
(16)

885 where $\mathbf{X}_u | \mathbf{Y}$ represents class-controlled features and $d(\cdot)$ denotes a distance function.

891 All of these feature homophily metrics measure the feature consistency, which still suffer from the
892 “good heterophily” issue as similar as node homophily or edge homophily. Our proposed Topologi-
893 cal Feature Informativeness (TFI) addresses this limitation by the mutual information, which better
894 aligns with GNNs performance on each feature in graphs.

895 **Heterophily-oriented GNNs** For graphs with low homophily (heterophily), GNNs are likely to
896 fail and even worse than non-GNNs models (Luan et al., 2024a). Therefore, many approaches
897 (Wang et al., 2024b; Yang et al., 2021b; Zheng et al., 2024b; Lu et al., 2024b; Luan et al., 2024c) are
898 proposed to improve the performance of GNNs on heterophilous graphs, which can be categorized
899 into graph level, node level, or feature level-based GNNs.

901 For the graph level, FAGCN (Bo et al., 2021) introduces high frequency signals in graph convolution
902 to capture local information to address heterophily. Similarly, ACMGCN (Luan et al., 2022a) and
903 FB-GNNs (Luan et al., 2022b) proposes filterbanks to fuse identify, low-pass, and high-pass filter
904 signals. To mitigate the limitation of local heterophilous neighbors, Mixhop (Abu-El-Haija et al.,
905 2019) and H2GCN Zhu et al. (2020b) introduces multi-hop neighbors during the graph convolution.
906 To extends the local neighbors in heterophilous graphs to global neighbors, GloGNN (Li et al., 2022)
907 proposes signed and learnable coefficient matrix and Geom-GCN (Pei et al., 2020b) introduces new
908 neighbors from the space of geometric embeddings.

909 For the node level, SnoH (Wang et al., 2024b) modifies the message propagation for each node with
910 varying receptive field in graph convolution. Similarly, CO-GNN (Finkelshtein et al., 2023) assigns
911 each node with different types of directed message propagation in a cooperative manner, NoSAF
912 (Wang et al., 2024c) provides each node with a node-specific layer aggregation with varying filter
913 weights, and Node-MOE (Han et al., 2024) identifies heterophilous nodes with a feature inconsis-
914 tency measurement, then treats these nodes differently with different filters. Different from these
915 approaches, DisamGCL (Zhao et al., 2024) adopts a contrastive learning objective, by identifying
916 ambiguous nodes with historical label predictions and treating these nodes as negative samples.

917 To our best knowledge, only DMP (Yang et al., 2021b) proposes to treat each feature differently
in heterophily-oriented GNNs. DMP first defines the attribute homophily as feature consistency

918 across the graph topology, then use a learnable weight to automatic learn the layer-wised weights
 919 for each features. However, this kind of attribute homophily suffers from "good heterophily" issue
 920 (Ma et al., 2021) and these homophily values haven't been used to guide the feature selection in
 921 graphs. Furthermore, these learnable weights in GNNs for feature selection still inferior than our
 922 statistic-based metrics, TFI.

924 B PROOF OF THEOREM 1

926 **Theorem 1.** Given a graph $\mathcal{G} = \{\mathcal{V}, \mathcal{E}\}$ with node features $\mathbf{X}_m \in \mathbb{R}^N$ in the m -th dimension and
 927 uniform node labels $\mathbf{Y} \in \mathbb{R}^N$ over \mathcal{V} , we can obtain aggregated features by applying graph con-
 928 volution k times, i.e., $\tilde{\mathbf{X}}_m = (\hat{\mathbf{A}})^k \mathbf{X}_m$. For a classifier that predicts label Y using the aggregated
 929 features \tilde{X}_m , its accuracy rate P_A is upper bounded by:

$$931 P_A \leq \frac{I(Y; \tilde{X}_m) + \log 2}{\log(C)} \quad (17)$$

934 *Proof.* For a node with its aggregated feature \tilde{X}_m , denote its true label as Y and the predicted label
 935 as $\hat{Y} = f(\tilde{X}_m)$, where $f(\cdot)$ represents the classifier. The occurrence of an error E in the classifier
 936 can be expressed as:

$$937 E := \begin{cases} 1 & \text{if } \hat{Y} \neq Y, \\ 0 & \text{if } \hat{Y} = Y. \end{cases} \quad (18)$$

940 Considering the Markov chain $Y \rightarrow \tilde{X} \rightarrow \hat{Y}$, we apply Fano's inequality (Gerchinovitz et al., 2020)
 941 to obtain:

$$942 H(Y|\tilde{X}) \leq H_b(P_E) + P_E \log(C - 1) \quad (19)$$

943 where P_E is the error rate and $H_b(\cdot)$ is the binary entropy function.

945 To express P_E , we rearrange the inequality:

$$946 P_E \geq \frac{H(Y|\tilde{X}) - H_b(P_E)}{\log(C - 1)} \quad (20)$$

949 Noting that $H(Y|\tilde{X}) = H(Y) - I(Y; \tilde{X}) = \log(C) - I(Y; \tilde{X})$ and that $H_b(P_E) \leq \log 2$, we can
 950 substitute these terms into the equation:

$$951 P_E \geq 1 - \frac{I(Y; \tilde{X}_m) + \log 2}{\log(C)} \quad (21)$$

955 Finally, converting the expression to the accuracy rate, we find:

$$956 P_A = 1 - P_E \leq \frac{I(Y; \tilde{X}_m) + \log 2}{\log(C)} \quad (22)$$

959 This concludes the proof.

962 C IMPLEMENTATION DETAILS

963 In this section, we provide all implementation details in Section 3 and Section 5. We have also made
 964 the code publicly available, which can be accessed here: [https://anonymous.4open.science/r/graph-
 965 feature-selection-BF28](https://anonymous.4open.science/r/graph-feature-selection-BF28).

968 C.1 DATASETS

969 We use Children, Computers, Fitness, History, Photo, Amazon-Ratings, Minesweeper, Questions,
 970 Roman-Empire, Tolokers as mentioned in Table 3 and Squirrel, Chameleon, Actor, Texas, Cornell,
 971 Wisconsin, Cora, CiteSeer, PubMed (?) as mentioned in Table 14 for all experiments. All datasets

Table 3: Dataset Statistics

Dataset	#Nodes	#Edges	#Features	#Classes	Ave. Degrees	Domain	Feat. Modeling	h_{node}	h_{edge}	h_{class}	h_{adj}	Avg. TFI
Children	76,875	1,554,578	768	24	20.22	E-commerce	PLMs	0.4579	0.4220	0.2372	0.2913	0.0225
Comp.	87,229	721,081	768	10	8.27	E-commerce	PLMs	0.8469	0.8322	0.7601	0.7988	0.0208
Fitness	173,055	1,773,500	768	13	10.25	E-commerce	PLMs	0.8991	0.9004	0.7940	0.8528	0.0366
History	41,551	358,574	768	12	8.63	E-commerce	PLMs	0.7812	0.6626	0.2654	0.5463	0.0296
Photo	48,362	500,939	768	12	10.36	E-commerce	PLMs	0.7792	0.7491	0.7229	0.6892	0.0234
Amazon.	24,492	93,050	300	5	3.80	E-commerce	FastText	0.3793	0.3804	0.1270	0.1357	0.0177
Mines.	10,000	39,402	7	2	3.94	Games	One-hot	0.6832	0.6828	0.0094	0.0108	0.0202
Questions	48,921	153,540	301	2	3.14	Website	FastText	0.8963	0.8396	0.0722	0.2759	0.0049
Roman.	22,662	32,927	300	18	1.45	Website	FastText	0.0415	0.0469	0.0230	-0.0778	0.4870
tolokers	11,758	519,000	10	2	44.14	Social	Statistics	0.6331	0.5945	0.1867	0.0887	0.0044

used in this work are in compliance with the MIT license. Tables 3 and 14 shows the dataset statistics and the values of homophily metrics measured on these datasets. The detailed definition of these homophily measurements are shown in Appendix A. The descriptions of main datasets are given below:

- Children and History (Yan et al., 2023) datasets are derived from the Amazon-Books dataset, consisting of items with the second-level label “Children” and “History”, respectively. In both datasets, nodes represent books, and edges indicate frequent co-purchases or co-views between books. Each book’s label corresponds to its third-level category. The node attributes are derived from the book’s title and description using Pre-trained Language Models (PLMs). The task is to classify the books into 24 categories for Children and 12 categories for History. More details can be found on: <https://github.com/sktsherlock/TAG-Benchmark>.
- Computers and Photo (Yan et al., 2023) datasets are extracted from the Amazon-Electronics dataset, including products with the second-level label “Computers” and “Photo”, respectively. Nodes in these datasets represent electronics products, and edges signify frequent co-purchases or co-views. The labels correspond to the third-level category of the products. User reviews embedded by PLMs were used as the text attributes of the nodes, with the review having the highest number of votes being selected, or, if such a review was unavailable, a random review was chosen instead. The task is to classify the products into 10 categories for Computers and 12 categories for Photo. More details can be found on: <https://huggingface.co/datasets/Sherirto/CSTAG/tree/main>.
- Fitness dataset (Yan et al., 2023) is derived from the Amazon-Sports dataset, consisting of fitness-related items with the second-level label “Fitness”. Nodes represent fitness products, and edges indicate frequent co-purchases or co-views between products, encoded by PLM. The labels are based on the third-level category, and the task is to classify items into 13 categories. More details can be found on: <https://huggingface.co/datasets/Sherirto/CSTAG/tree/main/Fitness>.
- Amazon-Ratings (Platonov et al., 2023) is derived from the Amazon product co-purchasing network metadata, provided by the SNAP (Leskovec & Krevl, 2014) Datasets, which nodes represent products and edges connect products that are frequently bought together. Node features are created using the mean of fastText (Grave et al., 2018) embeddings from product descriptions. The task is to predict the average rating of a product, grouped into five classes. More details can be found on: <https://github.com/yandex-research/heterophilous-graphs/tree/main/data>.
- Minesweeper (Platonov et al., 2023) is inspired by the classic Minesweeper game and is synthetic in nature. It consists of a regular 100x100 grid, where each node represents a cell connected to its eight neighboring cells (except for cells on the edges, which have fewer neighbors). In this setup, 20% of the nodes are randomly designated as mines. Each node has one-hot-encoded features representing the number of neighboring mines, with 50% of the nodes having missing features, indicated by a separate binary attribute. The task to recognize if a nodes is mine or not. More details can be found <https://github.com/yandex-research/heterophilous-graphs/tree/main/data>.
- Questions (Platonov et al., 2023) is based on user interactions on the Yandex Q question-answering platform. Nodes’ labels represent users, and edges connect users if one answered the other’s question during a one-year period. Node features are the mean of fastText (Grave et al., 2018) embeddings from user descriptions, with an additional binary

feature indicating users without descriptions. The task is to predict which users remained active (i.e., not deleted or blocked) at the end of the period. More details can be found <https://github.com/yandex-research/heterophilous-graphs/tree/main/data>.

- Roman-Empire (Platonov et al., 2023) is constructed from the “Roman Empire” article in the English Wikipedia. Nodes in the graph represent individual words in the article, and edges connect words that either appear consecutively in the text or are related via syntactic dependencies. The node’s class is syntactic role obtained using spaCy (Honnibal et al., 2020), and fastText (Grave et al., 2018) are used for word embeddings of node features. More details can be found <https://github.com/yandex-research/heterophilous-graphs/tree/main/data>.
- Tolokers (Platonov et al., 2023) is based on data from the Toloka crowdsourcing platform (Likhobaba et al., 2023). The nodes represent tolokers (workers) who have participated in at least one of 13 projects and edges connect workers who have collaborated on the same task. Node features are based on profile information and task performance statistics. The task is to predict which tolokers have been banned from a project. More details can be found <https://github.com/yandex-research/heterophilous-graphs/tree/main/data>.

For all datasets, we randomly split the train, validation, and test set as 50% : 25% : 25% for 10 runs. Specifically, to investigate the impact of supervision percentage on the performance of GFS, in Figure 6, we combine the train, validation and test sets for TFI calculation with a given ratio r .

C.2 MODEL

The details of all the GNN methods used in our experiments are introduced as follows:

- GCN (Kipf & Welling, 2016) performs a layer-wise propagation of node features and aggregates features from neighboring nodes to capture local graph structures. Each layer of the network updates the node embeddings by applying a convolution operation over the graph, which combines the node’s own features with the features of its neighbors. The authors’ implementation is available at <https://github.com/tkipf/gcn>.
- GAT (Velicković et al., 2017) leverages self-attention mechanisms to perform node classification on graph-structured data. The innovation of GAT lies in its ability to learn different attention coefficients for each neighboring node dynamically. Specifically, the attention coefficient between node i and its neighbor j is computed as: $e_{ij} = \text{LeakyReLU}(\mathbf{a}^T [W\mathbf{h}_i \| W\mathbf{h}_j])$, where \mathbf{h}_i and \mathbf{h}_j are the feature vectors of nodes i and j , W is a shared weight matrix, and \mathbf{a} is a learnable attention vector. The coefficients are normalized using the softmax function: $\alpha_{ij} = \frac{\exp(e_{ij})}{\sum_{k \in \mathcal{N}_i} \exp(e_{ik})}$, where \mathcal{N}_i denotes the set of neighbors of node i . The final node representation is computed as a weighted sum of its neighbors’ features: $\mathbf{h}'_i = \sigma(\sum_{j \in \mathcal{N}_i} \alpha_{ij} W\mathbf{h}_j)$. The multi-head attention mechanism improves stability and expressiveness by concatenating or averaging the outputs of multiple independent attention heads, which is set with `num_heads = 8` in our experiments. This allows GAT to assign different importances to each neighboring node while maintaining computational efficiency. The authors’ implementation is available at <https://github.com/PetarV-/GAT>.
- SAGE (Hamilton et al., 2017) introduces an inductive framework for node embeddings by aggregating features from a node’s local neighborhood rather than requiring all nodes to be available during training. Its key innovation lies in the aggregation functions that can efficiently generate embeddings for unseen nodes. The aggregation process involves sampling and aggregating feature information from a node’s neighborhood at each layer of the network. The general form of feature aggregation is: $h_v^{(k)} = \sigma(W^{(k)} \cdot \text{AGGREGATE}(h_u^{(k-1)}, \forall u \in \mathcal{N}(v)))$, where $\mathcal{N}(v)$ represents the set of neighbors of node v , and AGGREGATE is set to mean operation in our experiment. This allows the model to generalize across evolving graphs and unseen nodes. The authors’ implementation is available at <https://github.com/williamleif/GraphSAGE>.
- GT (Shi et al., 2020) is a transformer-based architecture designed for graph learning. It adapts the traditional Transformer model to graph data by incorporating node and edge

features into the attention mechanism. The key innovation of GT is the use of multi-head attention to propagate node features across graph edges while also considering edge information. In our experiments, we employ the Graph Transformer with 8 attention heads. The attention coefficients are calculated as: $\alpha_{ij} = \frac{\exp(\text{LeakyReLU}(\mathbf{q}_i^\top \mathbf{k}_j + \mathbf{e}_{ij}))}{\sum_{k \in \mathcal{N}(i)} \exp(\text{LeakyReLU}(\mathbf{q}_i^\top \mathbf{k}_k + \mathbf{e}_{ik}))}$, where \mathbf{q}_i and \mathbf{k}_j are the query and key vectors for nodes i and j , and \mathbf{e}_{ij} represents the edge feature between nodes i and j . This allows the model to aggregate both node and edge information. The author’s implementation is available at https://github.com/PaddlePaddle/PGL/tree/main/ogb_examples/nodeproppred/unimp

- SGC (Simplifying Graph Convolution) (Wu et al., 2019a) is a simplified variant of GCN designed to reduce computational complexity while maintaining similar performance. SGC removes the non-linear activation functions between layers of a traditional GCN, collapsing multiple layers into a single linear transformation. This reduces the overall complexity of the model and results in faster training and inference times. The propagation of node features in SGC can be expressed as: $\mathbf{H} = \mathbf{S}^K \mathbf{X} \mathbf{W}$, where \mathbf{S} is the normalized adjacency matrix, \mathbf{X} is the input feature matrix, \mathbf{W} is the weight matrix, and K is the number of propagation steps (or layers). By precomputing $\mathbf{S}^K \mathbf{X}$, the model reduces to simple logistic regression on the preprocessed features, significantly speeding up the training process. In our experiments, we use $K = 1$ for optimal performance. The authors’ implementation is available at <https://github.com/Tiiiger/SGC>.
- APPNP (Gasteiger et al., 2018) builds upon Graph Convolutional Networks (GCNs) by utilizing personalized PageRank for improved propagation of node features while avoiding oversmoothing. The model separates the neural network prediction from the propagation process, allowing it to handle larger neighborhood sizes efficiently. The propagation is controlled by the following iterative equation: $Z^{(k+1)} = (1 - \alpha) \hat{A} Z^{(k)} + \alpha H$, where \hat{A} is the normalized adjacency matrix, α is the teleport probability (set as $\alpha = 0.1$ in our experiments), and H is the initial node feature set. After k (set default $k = 2$) propagation steps, the output node features are computed as: $Z = \text{softmax}(Z^{(k)})$. This structure permits the model to aggregate information from both local and distant nodes without increasing the depth of the neural network. The authors’ implementation is available at <https://github.com/klicperajo/ppnp>.
- ACMGCN (Luan et al., 2022a) addresses the heterophily problem in graph neural networks (GNNs) by introducing an Adaptive Channel Mixing (ACM) framework. This model adapts to both homophilic and heterophilic graphs by dynamically learning to balance information from three channels: aggregation, diversification, and identity. The key innovation lies in its ability to adaptively learn different weights for each node, allowing the model to exploit local graph structure and node feature similarities. The three channels are combined using learned weights, allowing the model to emphasize different types of information for different nodes: $H^{(l)} = \alpha_L H_L^{(l)} + \alpha_H H_H^{(l)} + \alpha_I H_I^{(l)}$, where $H_L^{(l)}$, $H_H^{(l)}$, and $H_I^{(l)}$ represent the low-pass (aggregation), high-pass (diversification), and identity channels, respectively, and α_L , α_H , α_I are learned weights that balance these channels. This flexible channel mixing enables ACMGCN to significantly outperform standard GNN models on heterophilic graphs while maintaining strong performance on homophilic graphs. The authors’ implementation is available at <https://github.com/SitaoLuan/ACM-GNN>.
- FAGCN (Bo et al., 2021) tackles the limitation of traditional GNNs that primarily focus on low-frequency signals. FAGCN introduces a self-gating mechanism to adaptively combine both low-frequency and high-frequency signals, allowing it to handle both assortative and disassortative networks effectively. The key innovation is its ability to dynamically adjust the contribution of each frequency type in the message-passing process. The aggregation of node features is expressed as: $h_i^l = \epsilon h_i + \sum_{j \in \mathcal{N}(i)} \alpha_{Lij} (F_L h_j) + \alpha_{Hij} (F_H h_j)$, where F_L and F_H are low-pass and high-pass filters, respectively, and α_{Lij} and α_{Hij} are the learned attention coefficients for each type of signal. This enables FAGCN to adapt to different graph structures and alleviates the over-smoothing problem common in deep GNNs. The authors’ implementation is available at <https://github.com/bdy9527/FAGCN>.

C.3 TRAINING DETAILS

All models are implemented using the PyTorch (Ansel et al., 2024) framework and the DGL (Wang et al., 2019) library. We run experiments on a machine with 4 NVIDIA RTX A6000 GPUs, each with 48GB of memory. For most of the tables and figures illustrated in Section 5, we perform a grid search on all dataset and the hyperparameters used for search are list as follow:

- Number of layers: $\{2, 3\}$
- Hidden dimension: $\{128, 256, 512\}$
- Learning rate: $\{3 \times 10^{-5}, 10^{-4}, 3 \times 10^{-4}, 10^{-3}, 3 \times 10^{-3}, 10^{-2}\}$
- Weight decay: $\{0, 10^{-5}, 10^{-3}\}$
- Dropout rate: $\{0.1, 0.2, 0.4, 0.6, 0.8\}$

Specially, for response of GCN+GFS, GCN, and MLP to number of layers and hidden dimension, as shown in Figure 5 and Figure 11, the hyperparameters range of set are list as follow:

- Number of layers: $\{1, 2, 3, 4, 5, 6, 7, 8, 9, 10\}$
- Hidden dimension: $\{16, 32, 64, 128, 256, 512, 1024\}$
- Learning rate: $\{10^{-5}, 3 \times 10^{-5}, 10^{-4}, 3 \times 10^{-4}, 10^{-3}, 3 \times 10^{-3}, 10^{-2}, 3 \times 10^{-2}\}$
- Weight decay: $\{0, 10^{-5}, 3 \times 10^{-5}, 10^{-4}, 3 \times 10^{-4}, 10^{-3}\}$
- Dropout rate: $\{0.1, 0.2, 0.3, 0.4, 0.5, 0.6, 0.7, 0.8, 0.9\}$

To enhance the performance of all GNN models, we use skip connections (He et al., 2016) and layer normalization (Ba et al., 2016) across all methods.

Table 4: Hyperparameters for GNN baselines and GNN+GFS on Children.

Dataset	Model	Num of Layers	Hidden Dim	Learning Rate	Weight Decay	Dropout
Children	GCN	2	256	3e-3	1e-3	0.2
	GCN+GFS	2	256	3e-4	1e-4	0.2
	GAT	2	512	3e-5	0	0.2
	GAT+GFS	3	512	3e-4	0	0.2
	SAGE	2	512	3e-5	0	0.2
	SAGE+GFS	2	512	3e-5	0	0.2
	GT	2	512	3e-4	1e-3	0.2
	GT+GFS	3	512	3e-4	0	0.4
	SGC	2	512	3e-3	0	0.2
	SGC+GFS	2	512	3e-3	0	0.2
	APPNP	2	512	3e-5	0	0.2
	APPNP+GFS	2	512	3e-3	0	0.2
	ACMGCN	2	512	3e-5	0	0.2
	ACMGCN+GFS	3	512	3e-4	0	0.6
	FAGCN	2	512	3e-5	0	0.2
	FAGCN+GFS	2	512	3e-3	0	0.2

C.4 OPTIMIZATION-BASED GRAPH FEATURE SELECTION

We implement optimization-based metrics θ_{Soft} and θ_{Hard} mentioned in Section 5.

- θ_{Soft} : We use two learnable weight matrices, $\mathbf{W}_{\text{GNN}} \in \mathbb{R}^M$ and $\mathbf{W}_{\text{MLP}} \in \mathbb{R}^M$, to guide feature selection for GNN and MLP. For the input node features $\mathbf{X} \in \mathbb{R}^{N \times M}$, we divide them into a GNN-favored part $\mathbf{X}_{\mathcal{G}}$ and a GNN-disfavored part $\mathbf{X}_{-\mathcal{G}}$, computed as follows:

$$\mathbf{X}_{\mathcal{G}} = \frac{\mathbf{W}_{\text{GNN}}^2}{\mathbf{W}_{\text{GNN}}^2 + \mathbf{W}_{\text{MLP}}^2 + \epsilon} \cdot \mathbf{X} \quad (23)$$

$$\mathbf{X}_{-\mathcal{G}} = \frac{\mathbf{W}_{\text{MLP}}^2}{\mathbf{W}_{\text{GNN}}^2 + \mathbf{W}_{\text{MLP}}^2 + \epsilon} \cdot \mathbf{X} \quad (24)$$

1188

1189

Table 5: Hyperparameters for GNN baselines and GNN+GFS on Computers.

1190

1191

Dataset	Model	Num of Layers	Hidden Dim	Learning Rate	Weight Decay	Dropout
Computers	GCN	2	512	3e-5	0	0.2
	GCN+GFS	3	512	1e-4	3e-5	0.2
	GAT	2	128	3e-3	0	0.2
	GAT+GFS	3	512	3e-4	0	0.4
	SAGE	2	512	3e-5	0	0.2
	SAGE+GFS	3	512	3e-4	0	0.4
	GT	2	512	3e-5	0	0.2
	GT+GFS	3	512	3e-5	0	0.2
	SGC	3	512	3e-4	0	0.2
	SGC+GFS	3	512	3e-3	0	0.2
	APPNP	2	512	3e-5	0	0.2
	APPNP+GFS	3	512	3e-4	0	0.2
	ACMGCN	2	512	3e-5	0	0.2
	ACMGCN+GFS	3	512	3e-4	0	0.4
	FAGCN	2	512	3e-5	0	0.2
FAGCN+GFS	3	512	3e-3	0	0.2	

1205

1206

1207

Table 6: Hyperparameters for GNN baselines and GNN+GFS on Fitness.

1208

1209

Dataset	Model	Num of Layers	Hidden Dim	Learning Rate	Weight Decay	Dropout
Fitness	GCN	2	512	3e-5	0	0.2
	GCN+GFS	3	512	3e-4	0	0.2
	GAT	2	128	3e-3	0	0.2
	GAT+GFS	3	512	3e-4	0	0.2
	SAGE	2	512	3e-5	0	0.2
	SAGE+GFS	3	512	3e-4	0	0.2
	GT	2	512	3e-5	0	0.2
	GT+GFS	3	512	3e-4	0	0.2
	SGC	2	512	3e-3	0	0.2
	SGC+GFS	3	512	3e-3	0	0.2
	APPNP	2	512	3e-5	0	0.2
	APPNP+GFS	3	512	3e-4	0	0.6
	ACMGCN	2	512	3e-5	0	0.2
	ACMGCN+GFS	3	512	3e-4	0	0.6
	FAGCN	2	512	3e-5	0	0.2
FAGCN+GFS	2	512	3e-3	0	0.2	

1223

1224

1225

Table 7: Hyperparameters for GNN baselines and GNN+GFS on History.

1226

1227

Dataset	Model	Num of Layers	Hidden Dim	Learning Rate	Weight Decay	Dropout
History	GCN	2	256	3e-3	0	0.4
	GCN+GFS	2	512	3e-5	0	0.2
	GAT	2	512	3e-5	0	0.2
	GAT+GFS	2	512	3e-5	0	0.2
	SAGE	2	512	3e-5	0	0.2
	SAGE+GFS	2	512	3e-5	0	0.2
	GT	2	512	3e-5	0	0.2
	GT+GFS	3	512	3e-4	0	0.2
	SGC	2	256	3e-3	0	0.2
	SGC+GFS	3	512	3e-3	0	0.2
	APPNP	2	512	3e-5	0	0.2
	APPNP+GFS	2	512	3e-3	0	0.2
	ACMGCN	2	512	3e-4	0	0.2
	ACMGCN+GFS	2	512	3e-4	0	0.6
	FAGCN	2	512	3e-5	0	0.2
FAGCN+GFS	3	512	3e-3	0	0.2	

1241

1242

1243

Table 8: Hyperparameters for GNN baselines and GNN+GFS on Photo.

1244

1245

1246

1247

1248

1249

1250

1251

1252

1253

1254

1255

1256

1257

1258

1259

Dataset	Model	Num of Layers	Hidden Dim	Learning Rate	Weight Decay	Dropout
Photo	GCN	3	256	3e-3	0	0.4
	GCN+GFS	3	512	3e-5	0	0.2
	GAT	2	128	3e-3	0	0.2
	GAT+GFS	3	512	3e-4	0	0.2
	SAGE	2	512	3e-5	0	0.2
	SAGE+GFS	3	512	3e-4	0	0.2
	GT	3	512	3e-4	0	0.2
	GT+GFS	3	512	3e-5	0	0.2
	SGC	2	512	3e-3	1e-3	0.2
	SGC+GFS	3	512	3e-3	0	0.2
	APPNP	2	512	3e-5	0	0.2
	APPNP+GFS	3	512	3e-4	0	0.4
	ACMGCN	2	512	3e-3	0	0.4
	ACMGCN+GFS	3	512	3e-4	0	0.6
	FAGCN	2	512	3e-5	0	0.2
FAGCN+GFS	3	512	3e-3	0	0.2	

1260

1261

Table 9: Hyperparameters for GNN baselines and GNN+GFS on Amazon-Ratings.

1262

1263

1264

1265

1266

1267

1268

1269

1270

1271

1272

1273

1274

1275

1276

1277

Dataset	Model	Num of Layers	Hidden Dim	Learning Rate	Weight Decay	Dropout
Amazon-Ratings	GCN	2	512	3e-4	1e-3	0.4
	GCN+GFS	2	512	1e-3	1e-3	0.4
	GAT	2	512	3e-5	0	0.2
	GAT+GFS	3	512	3e-4	0	0.4
	SAGE	2	512	3e-5	0	0.2
	SAGE+GFS	3	512	3e-4	0	0.4
	GT	2	512	3e-5	0	0.2
	GT+GFS	3	512	3e-5	0	0.2
	SGC	3	512	3e-3	0	0.2
	SGC+GFS	2	512	3e-3	0	0.2
	APPNP	2	512	3e-5	0	0.2
	APPNP+GFS	2	512	3e-3	0	0.4
	ACMGCN	2	512	3e-4	0	0.4
	ACMGCN+GFS	3	512	3e-4	0	0.6
	FAGCN	2	512	3e-5	0	0.2
FAGCN+GFS	2	512	3e-3	0	0.2	

1278

1279

Table 10: Hyperparameters for GNN baselines and GNN+GFS on Minesweeper.

1280

1281

1282

1283

1284

1285

1286

1287

1288

1289

1290

1291

1292

1293

1294

1295

Dataset	Model	Num of Layers	Hidden Dim	Learning Rate	Weight Decay	Dropout
Minesweeper	GCN	2	512	3e-4	0	0.2
	GCN+GFS	2	128	1e-3	3e-4	0.2
	GAT	2	512	3e-4	0	0.2
	GAT+GFS	2	512	3e-5	0	0.2
	SAGE	2	512	3e-5	0	0.2
	SAGE+GFS	2	512	3e-5	0	0.2
	GT	2	512	3e-5	0	0.2
	GT+GFS	2	512	3e-5	0	0.2
	SGC	2	128	3e-3	0	0.2
	SGC+GFS	3	512	3e-3	0	0.2
	APPNP	2	512	3e-5	0	0.2
	APPNP+GFS	3	512	3e-4	0	0.2
	ACMGCN	3	512	3e-5	0	0.2
	ACMGCN+GFS	2	512	3e-5	0	0.2
	FAGCN	2	512	3e-5	0	0.2
FAGCN+GFS	3	512	3e-3	0	0.2	

1296

1297

Table 11: Hyperparameters for GNN baselines and GNN+GFS on Questions.

1298

1299

Dataset	Model	Num of Layers	Hidden Dim	Learning Rate	Weight Decay	Dropout
	GCN	2	512	3e-4	0	0.2
	GCN+GFS	3	128	1e-4	1e-3	0.2
	GAT	2	512	3e-4	0	0.2
	GAT+GFS	2	512	3e-5	0	0.2
	SAGE	2	512	3e-5	0	0.2
	SAGE+GFS	2	512	3e-5	0	0.2
	GT	2	512	3e-5	0	0.2
	GT+GFS	3	512	3e-5	0	0.4
Questions	SGC	3	512	3e-3	0	0.8
	SGC+GFS	3	512	3e-5	0	0.6
	APPNP	2	512	3e-5	0	0.2
	APPNP+GFS	3	512	3e-5	0	0.6
	ACMGCN	2	512	3e-5	0	0.2
	ACMGCN+GFS	2	512	3e-5	0	0.2
	FAGCN	2	512	3e-5	0	0.2
	FAGCN+GFS	3	512	3e-3	0	0.2

1313

1314

1315

Table 12: Hyperparameters for GNN baselines and GNN+GFS on Roman-Empire.

1316

1317

Dataset	Model	Num of Layers	Hidden Dim	Learning Rate	Weight Decay	Dropout
	GCN	2	512	3e-5	0	0.2
	GCN+GFS	3	128	1e-2	1e-4	0.3
	GAT	2	128	3e-3	0	0.4
	GAT+GFS	3	512	3e-4	0	0.6
	SAGE	2	512	3e-3	0	0.6
	SAGE+GFS	3	512	3e-4	0	0.4
	GT	2	512	3e-3	0	0.8
	GT+GFS	3	512	3e-4	0	0.6
Roman-Empire	SGC	2	128	3e-3	0	0.4
	SGC+GFS	2	512	3e-3	0	0.2
	APPNP	2	512	3e-5	0	0.2
	APPNP+GFS	2	512	3e-5	0	0.2
	ACMGCN	2	512	3e-3	0	0.8
	ACMGCN+GFS	3	512	3e-4	0	0.8
	FAGCN	2	512	3e-5	0	0.2
	FAGCN+GFS	2	512	3e-3	0	0.2

1331

1332

1333

Table 13: Hyperparameters for GNN baselines and GNN+GFS on Tolokers.

1334

1335

Dataset	Model	Num of Layers	Hidden Dim	Learning Rate	Weight Decay	Dropout
	GCN	2	512	3e-4	1e-5	0.2
	GCN+GFS	3	128	1e-3	3e-5	0.2
	GAT	2	512	3e-5	0	0.2
	GAT+GFS	3	512	3e-5	0	0.2
	SAGE	2	512	3e-5	0	0.2
	SAGE+GFS	3	512	3e-3	0	0.4
	GT	3	512	3e-5	0	0.2
	GT+GFS	3	512	3e-5	0	0.2
Tolokers	SGC	2	512	3e-3	0	0.2
	SGC+GFS	3	512	3e-3	0	0.2
	APPNP	2	512	3e-5	0	0.2
	APPNP+GFS	3	512	3e-3	0	0.2
	ACMGCN	3	512	3e-4	0	0.2
	ACMGCN+GFS	3	512	3e-4	0	0.2
	FAGCN	2	512	3e-5	0	0.2
	FAGCN+GFS	3	512	3e-3	0	0.2

1349

where ϵ is set to 10^{-7} to prevent division by zero. In this formulation, \mathbf{W}_{GNN} represents the proportion of each feature that is GNN-favored, while \mathbf{W}_{MLP} represents the proportion that is MLP-favored. The sum of $\mathbf{X}_{\mathcal{G}}$ and $\mathbf{X}_{-\mathcal{G}}$ equals the original input \mathbf{X} , indicating that the features are divided based on the relative influence of GNN and MLP preferences. These weight parameters are updated during the training process.

- θ_{Hard} : We use a learnable weight matrix, $\mathbf{W}_{\text{Hard}} \in \mathbb{R}^{M \times 2}$, to guide feature selection for GNN and MLP. For the input node features $\mathbf{X} \in \mathbb{R}^{N \times M}$, we divide them into a GNN-favored part $\mathbf{X}_{\mathcal{G}}$ and a GNN-disfavored part $\mathbf{X}_{-\mathcal{G}}$, computed as follows:

$$\mathbf{M}_{\text{Hard}} = \text{Gumbel-Softmax}(\mathbf{W}_{\text{Hard}}) \quad (25)$$

$$\mathbf{X}_{\mathcal{G}} = \mathbf{X} \cdot \mathbf{M}_{\text{Hard}}[:, 0] \quad (26)$$

$$\mathbf{X}_{-\mathcal{G}} = \mathbf{X} \cdot \mathbf{M}_{\text{Hard}}[:, 1] \quad (27)$$

In this case, $\mathbf{M}_{\text{Hard}} \in \mathbb{R}^{M \times 2}$ is the output of the Gumbel-Softmax applied to \mathbf{W}_{Hard} . For each row in \mathbf{M}_{Hard} , one value will be 1 and the other will be 0. A value of 1 indicates the selection of that feature, meaning that either the GNN-favored part or the MLP-favored part is chosen for each feature. This binary selection mechanism ensures that each feature is exclusively assigned to either $\mathbf{X}_{\mathcal{G}}$ or $\mathbf{X}_{-\mathcal{G}}$, depending on which component is favored. The use of Gumbel-Softmax(\cdot) (Jang et al., 2017) allows for differentiable sampling, enabling the weight parameters to be updated during the training process.

C.5 DETAILS OF PRETRAINED NODE EMBEDDINGS

We implement experiments using both GCN and MLP pretrained features to evaluate their effect when applying GCN+GFS on either the original node features, X , or on the pretrained node embeddings, $\text{MLP}(X)$ and $\text{GCN}(X, A)$. The results of this evaluation are presented in Figure 7 in the main text.

- $\text{MLP}(X)$: We pretrain a Multi-Layer Perceptron (MLP) model with the following setup: 2 layers, a hidden dimension of 128, trained for 1000 steps using the ELU activation function. For each of the 10 data splits, the MLP is trained separately with the Adam optimizer, using a learning rate of $1e-2$ and a weight decay of $5e-4$. The pretrained MLP is then used to extract $\text{MLP}(X)$ corresponding to the training splits, which serves as the node embeddings for the experiment.
- $\text{GCN}(X, A)$: We pretrain a Graph Convolutional Network (GCN) with 2 layers, a hidden dimension of 128, and trained for 1000 steps. The activation function used is ReLU, with a dropout rate of 0.5. Similarly, GCN is trained separately on each of the 10 data splits using the Adam optimizer, with a learning rate of $1e-2$ and a weight decay of $5e-4$. The pretrained GCN is then used to extract $\text{GCN}(X, A)$, corresponding to the training splits, as the node embeddings.

D MORE EXPERIMENTAL RESULTS

D.1 GCN+GFS ON ADDITIONAL DATASETS

We report the performance of GCN+GFS on additional datasets including Squirrel, Chameleon, Actor, Texas, Cornell, Wisconsin, Cora, CiteSeer, and PubMed. The dataset statistics and descriptions are shown in Figure 14.

Table 14: Additional Dataset Statistics

Dataset	#Nodes	#Edges	#Features	#Classes	Ave. Degrees	h_{node}	h_{edge}	h_{class}	h_{adj}	Avg. TFI
Squirrel	2223	46998	2089	5	21.14	0.1759	0.2072	0.0725	-0.0076	0.0173
Chameleon	890	8854	2325	5	9.95	0.2273	0.2361	0.0601	0.0360	0.0177
Actor	7600	26659	932	5	3.51	0.2197	0.2167	0.0074	0.0015	0.0029
Texas	183	279	1703	5	1.52	0.0748	0.0609	0.0017	-1.4628	0.0348
Cornell	183	277	1703	5	1.51	0.1246	0.1227	0.0482	-1.1984	0.0202
Wisconsin	251	450	1703	5	1.79	0.1934	0.1778	0.0447	-0.3947	0.0182
Cora	2708	10556	1433	7	3.90	0.8252	0.8100	0.7657	0.7717	0.0188
CiteSeer	3327	9228	3703	6	2.77	0.7166	0.7391	0.6267	0.6673	0.0103
PubMed	19717	88651	500	3	4.50	0.7924	0.8024	0.6641	0.6836	0.0440

As shown in Figure 9, the performance of the GCN+GFS model surpasses the standard GCN across additional datasets. The selective feature processing approach provided by GFS allows GNNs to focus on beneficial features, leading to improved performance across diverse datasets.

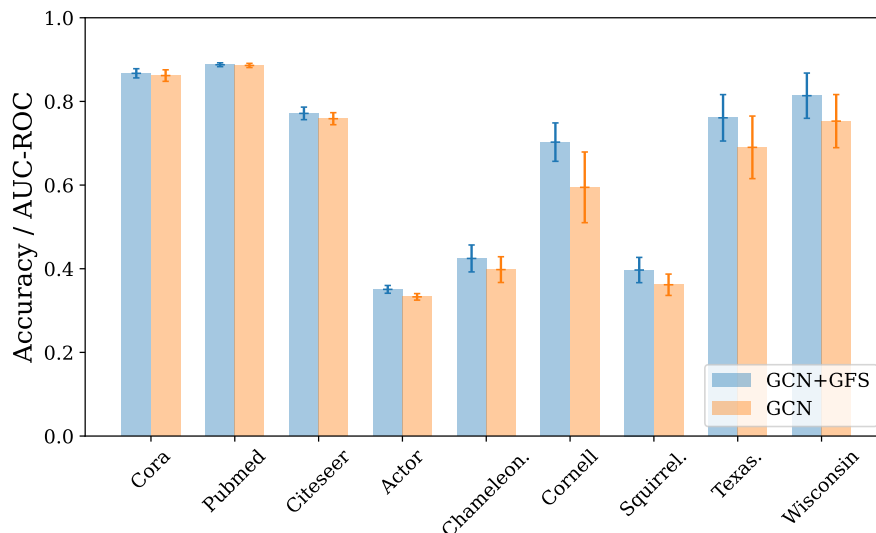


Figure 9: Performance on additional datasets.

D.2 SENSITIVITY OF GFS

Figure 10 shows the response of GCN+GFS to r on 6 other datasets, where GFS collapses to a GNN when $r = 1.0$ or an MLP when $r = 0.0$, as all features are sent to GNN or MLP, respectively. Although in some datasets like Minesweeper and Questions, where all the features may favor GNNs, GFS doesn't significantly improve GCN performance, it doesn't diminish GFS's overall effectiveness on most datasets.

Figure 11 shows how GCN, MLP, and GCN+GFS respond to changes in number of layers, dimension of hidden embeddings, learning rate, weight decay, and dropout rate on a homophilous graph (Computers) and a heterophilous graph (Amazon-Ratings) on other 6 datasets. In most cases, GFS outperforms GCN, but for certain hyperparameter settings on the Questions dataset, GFS does not consistently outperform GCN. This is likely because the node features in these datasets are already

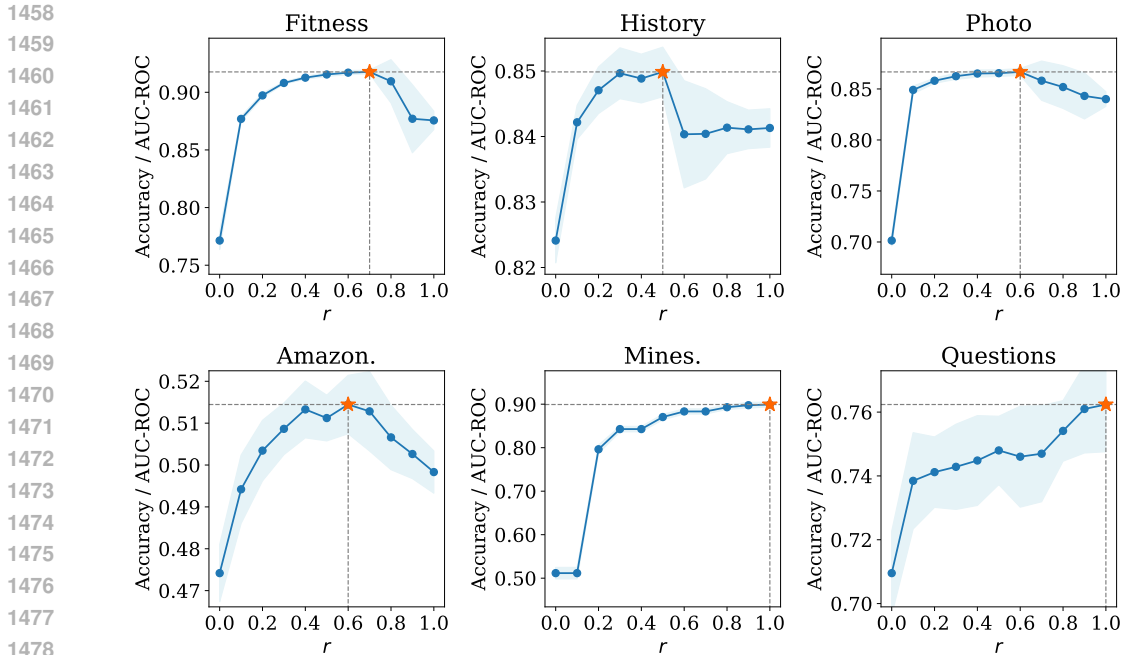


Figure 10: The performance of GCN+GFS is shown as the ratio r of GNN-favored features in TFI increases. The point representing the best performance is highlighted as \star .

highly graph-favored, making the additional feature selection offered by GFS less impactful. These results highlight the robustness of GFS under different hyperparameter settings.

D.3 PERCENTAGE OF SUPERVISION IN TFI

In Figure 12, the influence of the supervision percentage in TFI on the performance of GCN+GFS across other 6 datasets is shown. The results highlight that as the supervision percentage increases, the performance of GCN+GFS generally improves or stabilizes. Even with only 10% supervision, GCN+GFS outperforms the standard GCN, demonstrating the robustness of the TFI approach. For datasets like Fitness and Amazon, there is a noticeable improvement in performance as the supervision percentage increases, but it stabilizes at around 30%. In datasets such as History, Photos, and Mines, the model performance is relatively stable, indicating that a small percentage of supervision is sufficient to achieve optimal performance. The performance on Questions shows more variability with increasing supervision, possibly due to the graph-favored dataset’s features. This figure supports the claim that TFI requires minimal supervision to improve GCN+GFS performance, which is particularly useful in semi-supervised learning settings.

D.4 THE NUMBER OF K-HOP NEIGHBORS IN TFI

We further investigate the influence of the number of neighbor hops in TFI on the performance of GCN+GFS. We set k from $\{1, 2, \dots, 8\}$ as shown in Eq. (5). As illustrated in Figure 13, increasing the number of neighbor hops does not significantly affect model performance and results in only minor deviations in most datasets. This indicates that 1-hop neighbors are sufficient for TFI to select GNN-favored or GNN-disfavored features.

D.5 PERFORMANCE ON DATASETS WITH PUBLIC SPLITS

We further conduct the experiments on these datasets with public splits as shown in Table 15. Accuracy results on node classification are reported for Cora, PubMed, and CiteSeer, each having one split. For the other datasets, which have ten splits, we provide both accuracy and standard deviation.

The results demonstrate that GNN+GFS outperforms baseline GNN in most datasets for 4 types of GNN backbones, which include GCN, GAT, SGC, and GraphSAGE.

Table 15: The performance of graph feature selection on GNN baselines in public split datasets.

Model	Cora	Pubmed.	Citeseer	Actor	Chameleon.	Cornell	Squirrel	Texas.	Wisconsin
GCN	81.28	78.06	70.60	33.68±0.64	62.41±1.97	60.81±6.53	48.41±1.52	66.49±6.14	77.65±4.91
GCN+GFS	81.94	78.46	71.74	35.30±0.85	62.68±2.02	68.11±6.47	49.13±1.78	77.57±6.50	80.39±4.89
Δ	+0.66	+0.40	+1.14	+1.62	+0.27	+7.30	+0.72	+11.08	+2.74
GAT	80.16	76.92	69.88	33.07±0.79	65.79±2.55	63.24±4.97	51.63±1.47	74.05±4.97	76.47±3.70
GAT+GFS	81.06	77.94	72.24	35.23±0.83	66.49±2.11	69.19±5.87	52.15±1.83	77.84±4.38	81.57±6.21
Δ	+0.90	+1.02	+2.36	+2.16	+0.70	+5.95	+0.52	+3.79	+5.10
SGC	80.74	76.96	69.84	30.64±0.75	54.39±1.79	43.24±7.64	39.91±1.56	54.86±4.42	53.73±5.64
SGC+GFS	81.48	76.38	71.18	35.62±1.20	54.63±2.14	67.30±4.84	42.19±1.12	71.62±4.27	78.63±6.43
Δ	+0.74	-0.58	+1.34	+4.98	+0.24	+24.06	+2.28	+16.76	+24.90
SAGE	81.06	76.80	68.52	36.20±0.81	58.42±2.53	70.00±7.03	39.32±2.06	74.59±5.73	81.18±2.11
SAGE+GFS	81.88	78.40	71.46	36.47±0.72	58.71±1.93	71.08±5.70	39.28±1.49	81.08±5.55	83.14±5.08
Δ	+0.82	+1.60	+2.94	+0.27	+0.29	+1.08	-0.04	+6.49	+1.96

D.6 IMPACT OF LABEL HOMOPHILY

To investigate how GSF performs under varying label homophily, we conduct experiments on synthetic datasets using CSBM-H (Luan et al., 2024b; Zheng et al., 2024a) to control homophily levels. Specifically, in the CSBM-H model, for a node u labeled with y , its features $\mathbf{X}_u \in \mathbb{R}^M$ are sampled from a class-wise Gaussian distribution, specifically $\mathbf{X}_u \sim \mathcal{N}_{Y_u}(\mu_{Y_u}, \Sigma_{Y_u})$. Each dimension of \mathbf{X}_u is independent of each other. To construct the graph structure \mathcal{G} with a specified homophily degree h , the node u has a probability h of connecting to nodes with the same label and a probability of $\frac{1-h}{C-1}$ of connecting to nodes with different label. We randomly generate 10 graphs with different seeds in our experiments to reduce uncertainty. Each graph has 1000 nodes with 10 features and 5 classes. The node degrees are uniformly sampled from $[2, 8]$.

We demonstrate how the performance of GCN+GFS varies with label homophily across the range $[0.1, 0.2, \dots, 0.9]$ in Table 16 and Figure 14 for node classification tasks. Generally, GCN+GFS outperforms both GCN and MLP across different levels of label homophily, indicating that GFS addresses the limitations of GCN under low homophily and of MLP under high homophily through effective feature selection. Furthermore, the relative increase Δ (defined as the accuracy gap between GCN+GFS and GCN, divided by the accuracy of GCN) decreases as label homophily increases. This finding is expected, as higher homophily levels typically enhance the performance of all graph-aware models, thereby limiting the potential for improvement through GFS.

Table 16: Impact of label homophily on GFS.

Label Homophily	0.1	0.2	0.3	0.4	0.5	0.6	0.7	0.8	0.9
MLP	73.12±4.06	71.24±5.81	68.44±6.93	70.36±5.30	66.92±6.36	67.52±4.64	70.12±5.49	69.88±4.77	69.32±4.68
GCN	50.12±3.09	50.56±3.28	56.00±5.49	61.24±5.30	65.84±5.11	72.32±2.35	80.32±3.44	87.64±2.23	90.64±2.32
GCN+GFS	73.24±3.85	69.96±7.24	69.04±6.76	71.36±6.17	69.68±7.69	73.84±4.65	82.76±6.65	89.36±4.20	91.20±6.04
Δ (relative)	23.12%	19.40%	13.04%	10.12%	3.84%	1.52%	2.44%	1.72%	0.56%

D.7 IMPACT OF FEATURE DIMENSION

We investigate the impact of feature dimension size based on the CSBM-H model (Luan et al., 2024b; Zheng et al., 2024a), following the setup described in Section D.6. As shown in Table 17 and Figure 15, GFS demonstrates a pronounced advantage over GCN as the feature dimension increases. This outcome is expected, as more features allow GFS to exhibit higher fault tolerance during feature selection. In real-world scenarios, where the feature dimensions in datasets can reach hundreds or thousands, as indicated in Table 3, GFS is likely to perform well.

D.8 IMPACT OF FEATURE SPARSENESS

We investigate the impact of feature sparseness on the CSBM-H model (Luan et al., 2024b; Zheng et al., 2024a), following the setup outlined in Section D.6. To control sparseness in synthetic

Table 17: Impact of size of feature dim on GFS.

#Feature Dim	10	20	30	40	50
MLP	67.52±4.64	77.76±3.53	83.40±2.58	87.60±1.89	91.12±1.88
GCN	72.32±2.35	79.20±2.15	81.40±2.37	84.64±3.07	87.80±2.73
GCN-GFS	73.84±4.65	84.12±3.70	87.40±3.68	90.84±3.51	94.12±3.37
Δ (relative)	2.06%	5.85%	6.86%	6.83%	6.71%

datasets, we randomly mask a certain percentage of node features. As shown in Table 18 and Figure 16, the results indicate that the advantage of GFS diminishes as feature sparseness increases. Although the relative increase rate of GFS decreases in this context, it still outperforms GCN. This is attributed to the presence of both GNN-favored and GNN-disfavored features, which allows GFS to remain effective in enhancing GNN performance.

Table 18: Impact of sparseness on GFS.

Sparseness	0%	10%	20%	30%	40%	50%	60%	70%	80%	90%
GCN	54.16±5.58	46.48±3.79	48.88±3.43	45.68±1.93	42.12±2.88	39.52±2.86	34.88±5.59	32.08±2.05	29.92±2.75	25.12±3.07
GCN-GFS	67.96±7.72	59.84±6.83	60.04±5.49	54.92±5.47	50.64±4.15	46.20±5.26	39.52±6.72	35.68±3.05	31.36±5.09	27.24±3.65
Δ (relative)	25.48%	28.74%	22.83%	20.23%	20.23%	16.90%	13.30%	11.22%	4.81%	8.44%

D.9 IMPACT OF NOISES IN FEATURES

To investigate the impact of feature noise on GFS, we conduct experiments on four real-world datasets: Children, Computer, Roman-Empire, and Tolokers, by introducing noise to the original node features. Specifically, after normalizing the input features, we add Gaussian noise multiple times. As shown in Table 19 and Figure 17, the relative increase Δ (defined as the accuracy gap between GCN+GFS and GCN, divided by the accuracy of GCN) remains relatively stable, indicating that the performance of GFS is robust against feature noise.

Table 19: Impact of noise on GFS.

Datasets	Noise	1	5	10	15	20
Children	GCN	52.92±1.17	52.93±0.62	52.57±0.75	52.32±0.89	52.20±0.75
	GCN-GFS	58.16±1.82	57.56±2.64	57.01±3.24	56.31±3.78	55.87±3.94
	Δ (relative)	9.89%	8.75%	8.44%	7.65%	7.04%
Comp.	GCN	84.39±1.25	84.42±0.85	83.07±1.09	82.46±0.77	81.68±0.94
	GCN-GFS	88.87±2.82	88.50±2.25	87.80±3.17	87.10±3.40	85.01±5.18
	Δ (relative)	5.31%	4.84%	5.69%	5.63%	4.08%
Roman.	GCN	84.11±0.30	83.96±0.33	83.65±0.40	83.23±0.33	83.00±0.25
	GCN-GFS	84.85±0.80	84.57±0.77	84.19±0.92	83.73±0.91	83.59±0.83
	Δ (relative)	0.87%	0.73%	0.64%	0.60%	0.71%
Tolokers	GCN	82.83±1.41	83.28±0.73	82.81±0.79	82.50±0.77	82.12±0.62
	GCN-GFS	86.52±1.85	85.99±1.79	85.48±1.54	84.99±0.87	84.44±1.75
	Δ (relative)	4.46%	3.25%	3.23%	3.01%	2.81%

D.10 GOOD HETEROPHILY ON FEATURE HOMOPHILY

In this section, we show the phenomenon of "good heterophily" occurs in feature homophily. First, we split node features into 10 bins according to the values of feature homophily. Then, we run GCN on these bins separately to see how the model performance changes with feature homophily. As shown in Table 20 and Figure 18, the GCN performance remains good under a low value of feature homophily, which includes attribute homophily (Yang et al., 2021a) (h_{attr}), local similarity (Chen et al., 2023) ($h_{sim-euc}$), and class-controlled feature homophily (Lee et al., 2024) (h_{CTF}).

This result indicates these consistency-based feature homophily cannot align well with GNN performance, which is similar to the phenomenon in label homophily (Ma et al., 2021; Luan et al., 2024b; Zheng et al., 2024a). Conversely, GNN performance consistently increases with the increase of our proposed TFI, implying its effectiveness in selecting GNN-favored or GNN-disfavored features.

Table 20: GCN performance on different bins of feature homophily metrics.

Metrics	0.0-0.1	0.1-0.2	0.2-0.3	0.3-0.4	0.4-0.5	0.5-0.6	0.6-0.7	0.7-0.8	0.8-0.9	0.9-1.0
h_{attr}	31.94±0.16	31.51±0.95	30.26±4.82	30.21±4.76	30.02±4.99	30.07±3.95	29.34±4.30	30.85±2.59	29.96±3.90	31.40±2.26
$h_{sim-euc}$	31.92±0.18	29.52±5.15	31.13±2.02	31.21±1.61	30.75±3.65	30.16±4.75	31.38±1.40	31.19±1.86	31.22±1.61	30.89±3.10
h_{CTF}	31.94±0.16	31.43±0.94	30.31±4.46	30.55±3.37	30.79±2.97	31.55±0.92	30.08±4.67	31.31±1.78	30.75±2.75	31.92±1.74
TFI	31.94±0.16	35.24±1.02	37.43±1.63	37.44±1.36	41.04±0.70	43.22±0.55	44.28±0.60	45.13±0.30	45.12±0.33	45.67±0.34

D.11 STATISTICAL OF SELECTED FEATURES

As shown in Table 21, we present the statistics of values, sparsity, and TFI for all features, GNN-favored features, and GNN-disfavored features. The results indicate that: (1) the TFI of GNN-favored features is significantly higher than that of GNN-disfavored features; (2) the datasets encoded by Pretrained Language Models (PLMs), including Children, Computers, Fitness, History, and Photo, exhibit similar values in features, yet their TFI varies considerably. Notably, a higher average TFI across all features correlates with better GFS performance; (3) GFS is less effective on datasets with higher sparsity, such as Minesweeper and Tolokers. (4) Datasets with lower homophily tend to identify more features as GNN-disfavored, whereas those with higher homophily identify more features as GNN-favored.

Table 21: Summary Statistics of Values, TFI, and Sparseness for Selected Features.

Dataset	X			X_G			X_{-G}			r
	Value	Sparseness	TFI	Value	Sparseness	TFI	Value	Sparseness	TFI	
Children	0.0202±0.4081	0.00%	0.0278±0.0158	0.0202±0.4081	0.00%	0.0396±0.0143	0.0202±0.4082	0.00%	0.0159±0.0039	50%
Comp.	0.0201±0.4068	0.00%	0.0965±0.0232	0.0201±0.4063	0.00%	0.1010±0.0239	0.0202±0.4090	0.00%	0.0785±0.0021	80%
Fitness	0.0195±0.3928	0.00%	0.1841±0.0220	0.0195±0.3929	0.00%	0.1906±0.0233	0.0195±0.3927	0.00%	0.1688±0.0019	70%
History	0.0201±0.4039	0.00%	0.0412±0.0261	0.0201±0.4034	0.00%	0.0594±0.0258	0.0201±0.4044	0.00%	0.0230±0.0057	50%
Photo	0.0202±0.4066	0.00%	0.0680±0.0278	0.0201±0.4052	0.00%	0.0817±0.0285	0.0202±0.4088	0.00%	0.0475±0.0037	60%
Amazon.	0.0003±0.0573	0.00%	0.0914±0.0065	0.0003±0.0572	0.00%	0.0957±0.0040	0.0003±0.0575	0.00%	0.0850±0.0036	60%
Mines.	0.1429±0.3499	85.71%	0.0369±0.0384	0.1429±0.3499	85.71%	0.0510±0.0368	0.1429±0.3499	85.71%	0.0014±0.0014	80%
Questions	-0.0007±0.0510	15.18%	0.0074±0.0011	-0.0007±0.0510	15.19%	0.0077±0.0010	-0.0007±0.0504	15.09%	0.0055±0.0004	90%
Roman.	0.0006±0.0986	0.27%	0.0874±0.0396	0.0007±0.1015	0.15%	0.1520±0.0388	0.0006±0.0979	0.30%	0.0712±0.0167	20%
tolokers	0.3825±0.4567	48.03%	0.0295±0.0139	0.3826±0.4565	48.06%	0.0349±0.0135	0.3823±0.4570	47.98%	0.0169±0.0005	70%

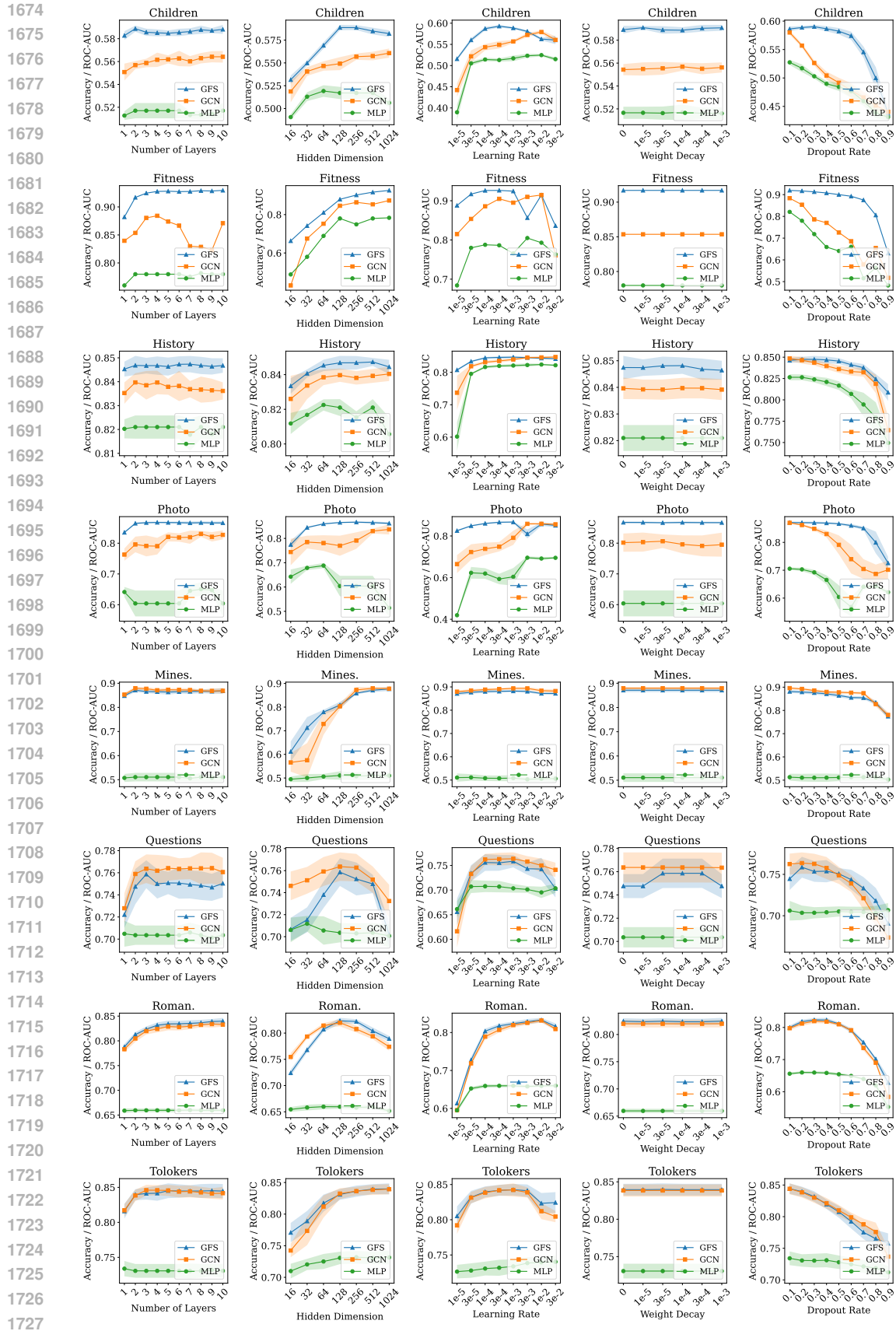


Figure 11: Response of GCN+GFS, GCN, and MLP to 5 hyperparameters on more datasets.

1728
1729
1730
1731
1732
1733
1734
1735
1736
1737
1738
1739
1740
1741
1742
1743
1744
1745
1746
1747
1748
1749
1750
1751
1752
1753
1754
1755
1756
1757
1758
1759
1760
1761
1762
1763
1764
1765
1766
1767
1768
1769
1770
1771
1772
1773
1774
1775
1776
1777
1778
1779
1780
1781

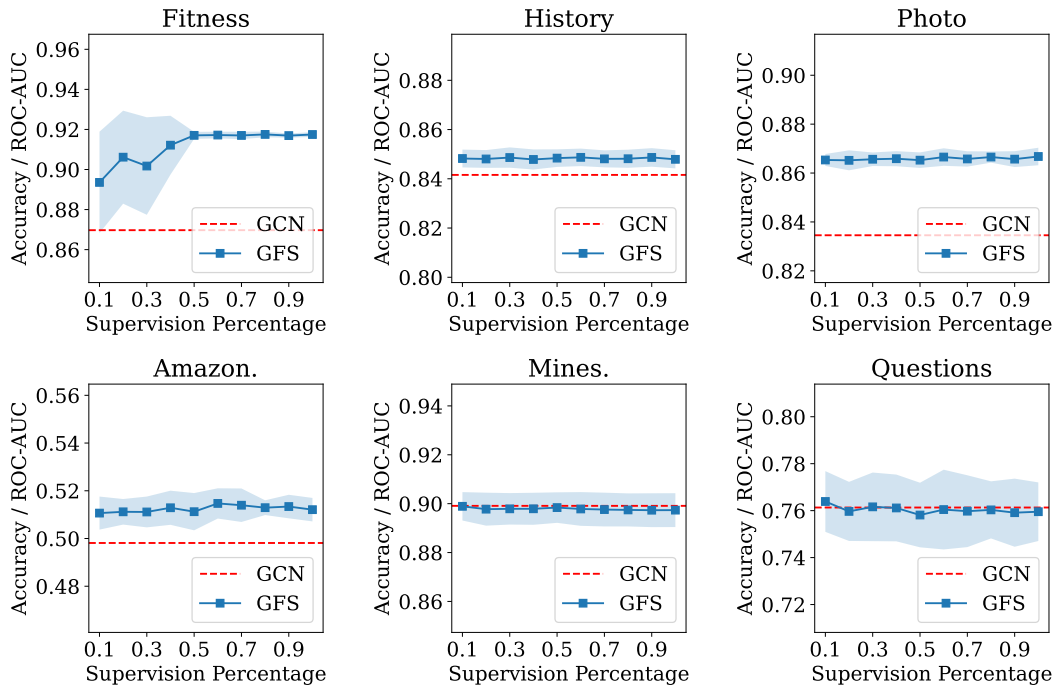


Figure 12: Influence of the percentage of the supervision in TFI on the model performance of GCN+GFS.

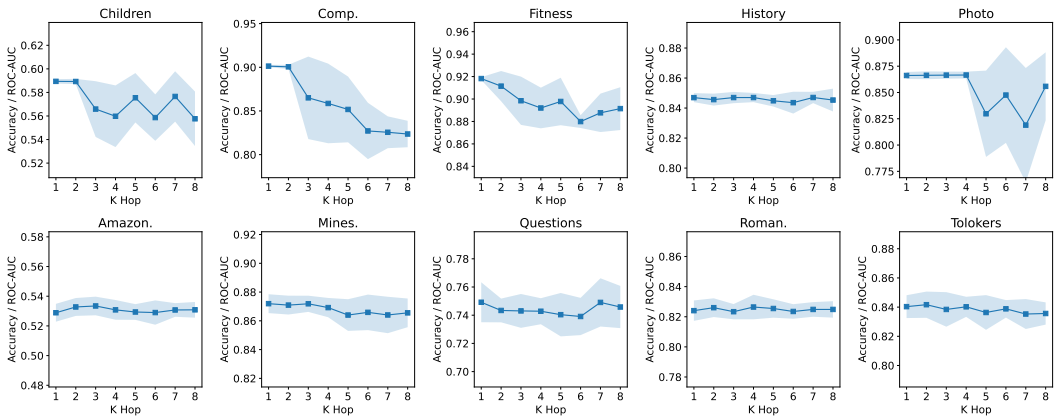


Figure 13: Influence of the number of neighbor hops in TFI on the performance of GCN+GFS.

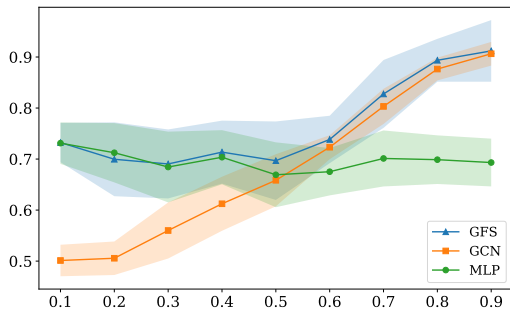


Figure 14: Comparison of the performance of MLP, GCN, and GFS across varying levels of label homophily in synthetic datasets.

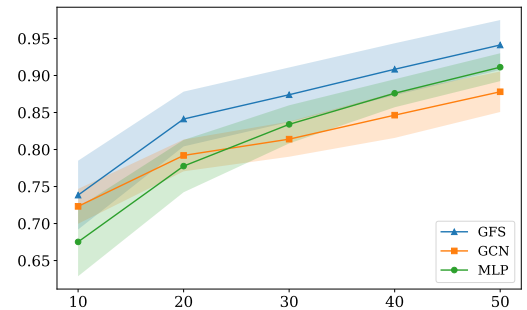


Figure 15: Comparison of the performance of MLP, GCN, and GFS with the increase of the number of feature dimensions.

1782
1783
1784
1785
1786
1787
1788
1789
1790
1791
1792
1793
1794
1795

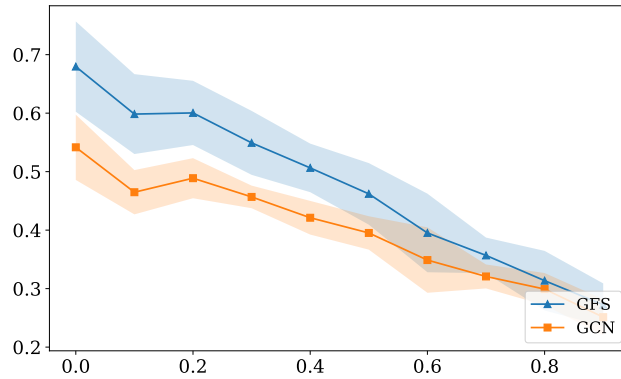


Figure 16: Comparison of the performance of MLP, GCN, and GFS with the sparseness in synthetic datasets

1796
1797
1798
1799
1800
1801
1802
1803
1804
1805
1806
1807

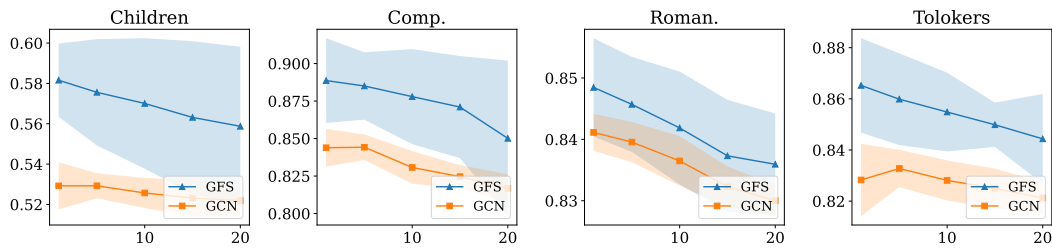


Figure 17: Comparison of the performance of MLP, GCN, and GFS with the increase of feature noises

1808
1809
1810
1811
1812
1813
1814
1815
1816
1817
1818
1819
1820
1821
1822
1823
1824
1825
1826
1827
1828
1829
1830
1831
1832
1833
1834
1835

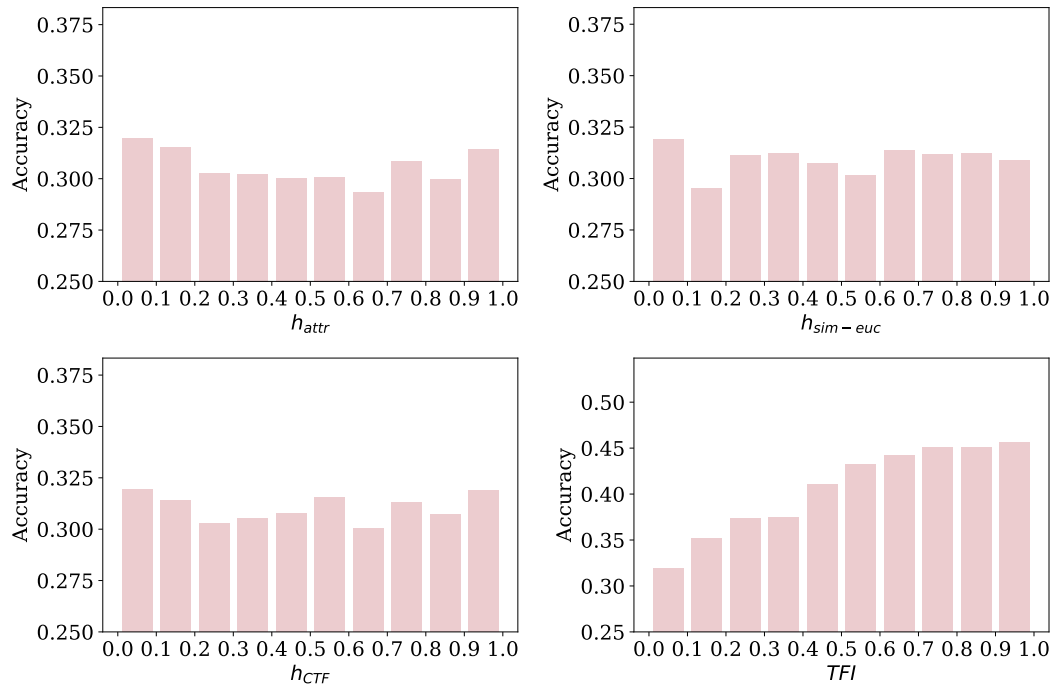


Figure 18: Performance of GCN under varying levels of feature homophily or TFI.

1836
1837
1838
1839
1840
1841
1842
1843
1844
1845
1846
1847
1848
1849
1850
1851
1852
1853
1854
1855
1856
1857
1858
1859
1860
1861
1862
1863
1864
1865
1866
1867
1868
1869
1870
1871
1872
1873
1874
1875
1876
1877
1878
1879
1880
1881
1882
1883
1884
1885
1886
1887
1888
1889

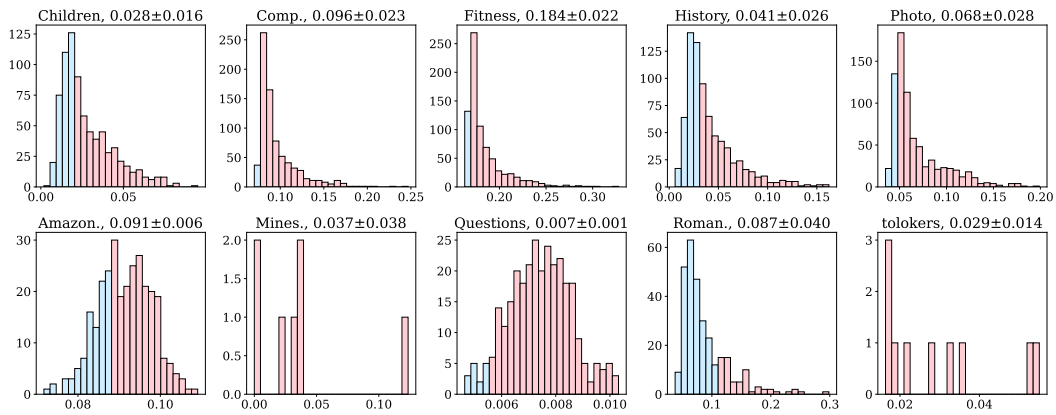


Figure 19: Visualizations of histogram of TFI on 10 datasets.